ISA Transactions 109 (2021) 269–287

Contents lists available at ScienceDirect

ISA Transactions

journal homepage: www.elsevier.com/locate/isatrans

Practice article

# An optimal filter length selection method for MED based on autocorrelation energy and genetic algorithms

Zhiyuan He [a], Guo Chen [a,*], Tengfei Hao [b], Xiyang Liu [a], Chunyu Teng [c]

[a] College of Civil Aviation, Nanjing University of Aeronautics and Astronautics, Nanjing, 211106, China
[b] School of Automotive & Rail Transit, Nanjing Institute of Technology, Nanjing 211167, China
[c] Innovative Research Center, China Aero-Polytechnology Establishment, Beijing 100028, China

ARTICLE INFO

*Article history:*
Received 8 February 2020
Received in revised form 13 August 2020
Accepted 4 October 2020
Available online 6 October 2020

*Keywords:*
Minimal Entropy Deconvolution (MED)
Filter length
Weak periodic impulses
Rolling bearings
Fault diagnosis

ABSTRACT

This paper proposed a method for exact selecting the optimal filter length of minimal entropy deconvolution (MED) to solve it recovering a single random pulse when the filter length is not improper. The energy ratio of autocorrelation between the filtered signal and the residual signal is adopted to measure the salience of periodic impulses. Then this index is used as an objective function of genetic algorithms (GA) to form an adaptive optimal selection method of filter length. The proposed method is verified by two different rolling bearing fault experiments. The results show that the proposed method reveals the periodic impulses successfully from the casing signals. Compared with other MED-based methods, the proposed method has better performance in detecting the weak fault signal.



## 1. Introduction

The failure of rolling bearing is one of the common causes of fault and accident in rotating machinery. Quasi-periodic or periodic impulses are considered as an important sign of rolling bearing fault [1]. Extracting periodic fault features from the vibration signal is a key step in the diagnosis process. However, owing to the noise interference of other mechanical components and the effect of the transmission path, the fault features of rolling bearings are very weak in some cases. In order to solve this problem, blind deconvolutions are introduced to recover the weak impact characteristics, among which Minimal Entropy Deconvolution (MED) is one of the classical methods.

MED was first proposed by Wiggins [2] to enhance the seismic reflection signal. It aims to maximize the kurtosis of weak impulses and minimize the kurtosis of other noise components. Sawalhi et al. [3] first demonstrated its effectiveness when applied to bearings fault detection. Subsequently, MED has been widely used in rotating machinery [4–6]. However, there are some problems with the MED. The goal of the filter is to maximize the kurtosis of the signal, but excessive kurtosis results in a single random large pulse. Besides, MED is very sensitive to the filter length, which will affect its output seriously. Some researchers were devoted to improving the objective function of the algorithm, such as changing kurtosis to skewness [7,8], correlation kurtosis (MCKD) [9], D-norm (OMEDA), multi-D-norm (MOMEDA) [10], impulse norm (MIND) [11] and autocorrelation impulse harmonic to noise (AIHN) [12] and so on. Other researchers focused on optimizing the filter coefficients in MED with some algorithms. For instance, Cheng et al. [13] combined the particle swarm optimization (PSO) algorithm with MED to optimize filter coefficients. Jiang et al. [14] proposed a method to optimize the filter coefficients of MED using the $l_0$-norm. These above methods have achieved remarkable results in bearing fault diagnosis.

However, there are few discussions on the exact selection of the filter length. When the filter length is not suitable, MED tends to change the periodic impulse component into a random single pulse component. Essentially, MED is a filter, so the above methods need to set the filter length in advance. The literature [15] shows that as the filter length is longer, the kurtosis value of the signal is larger, but in its research results, only a range of the filter length was obtained based on the experimental data, and there was no accurate filter length selection scheme. Refs. [13,16] used an empirical formula to determine the size of the filter length, but the scope of this formula is relatively rough. Li et al. [17] established the modified power spectrum kurtosis (MPSK) index to form an adaptive MED and successfully diagnosed the fault bearing of the wind turbine with the combination of time-delayed feedback monostable stochastic resonance. Nevertheless, the results of filtering are not very ideal and the effects of different filter lengths on fault signals are not discussed in detail. Besides, in

* Corresponding author.
*E-mail addresses:* hzy2017@nuaa.edu.cn (Z. He), cgzyx@263.net, hzy2017@nuaa.edu.cn (G. Chen).

https://doi.org/10.1016/j.isatra.2020.10.010
0019-0578/

some studies, when using the MED method for fault diagnosis, the filter length is obtained based on experience [18] or does not consider the effect of the filter length [19–21]. Therefore, a method of automatically selecting the optimal filter length of MED is proposed to enable the MED to enhance the periodic impulses as much as possible, and avoid causing a single random noise pulse. It uses the autocorrelation function to establish an energy determination index, which can measure the periodicity of fault characteristics for maximizing the separation of periodic impulses and noise. Then, taking the proposed index as an objective function, the optimal filter length is obtained by genetic algorithms (GA). Through the run-to-failure test of rolling bearing and the aero-engine rotor fault experiments that far away from the vibration source of the bearing, it is fully verified that the proposed method can enhance the weak fault features at the accurate filter length and avoid misdiagnosis caused by an inappropriate selection of the filter length. The main contribution of this paper is that we propose a method to accurately select the filter length of MED, which can improve the accuracy of MED in weak fault diagnosis, and give full play to the potential of MED in recovering the weak periodic impulse, especially when far away from the fault vibration source.

The structure of this paper is as follows: Section 2 reviews the algorithm of MED and shows the effects of different filter lengths on the outputs. Section 3 gives the detailed steps of the proposed method. Section 4 introduces two sets of rolling bearing fault experiments and verifies the effectiveness of the proposed method. Section 5 compares the results of the proposed method with PSO-MED and MCKD. Discussions and some conclusions are given in Section 6 and Section 7, respectively.

## 2. Minimal entropy deconvolution

### 2.1. Review of MED

As shown in Fig. 1, $\boldsymbol{s}$ is the fault periodic impulses, $\boldsymbol{n}$ is the noise, $\boldsymbol{h}$ represents the influence of system harmonics and transmission path. The observation signal $\boldsymbol{x}$ collected by the vibration sensor can be expressed as:

$$\boldsymbol{x} = (\boldsymbol{s} + \boldsymbol{n}) * \boldsymbol{h} \tag{1}$$

where * is the convolution, MED assumes that the system input $\boldsymbol{s}$ is a sparse pulse sequence, which has a small entropy value, but the entropy of $\boldsymbol{x}$ increases after passing through the system. So deconvolution is to find a finite impulse response (FIR) filter $\boldsymbol{f}$ whose length is $L$, and the $\boldsymbol{y}$ after the filter can approximate the input $\boldsymbol{s}$ of the original system, namely:

$$y(j) = \sum_{l=1}^{L} f(l)\, x(j-l) \approx s(j) \quad j = 1, 2, \ldots, N \tag{2}$$

The implementation of MED mainly includes the eigenvector method and objective function method. The objective function method is widely used, which can be realized by solving kurtosis, that is:

$$O_4[f(l)] = \sum_{j=1}^{N} y^4(j) \Big/ \left[\sum_{j=1}^{N} y^2(j)\right]^2 \tag{3}$$

$N$ is the length of data. The best filter can be obtained by making its first derivative is 0, namely:

$$\partial O_4[f(l)]/\partial f(l) = 0 \tag{4}$$

The matrix form of Eq. (2) is:

$$\boldsymbol{y} = \boldsymbol{X}_0^T \boldsymbol{f} \tag{5}$$

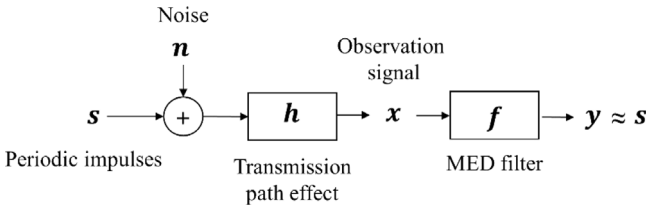


**Fig. 1.** The flows of blind deconvolution.

where: $\boldsymbol{X}_0 = \begin{bmatrix} x_1 & x_2 & x_3 & \cdots & \cdots & x_N \\ 0 & x_1 & x_2 & \cdots & \cdots & x_{N-1} \\ 0 & 0 & x_1 & \cdots & \cdots & x_{N-2} \\ \vdots & \vdots & \vdots & \ddots & \cdots & \vdots \\ 0 & 0 & 0 & \cdots & \cdots & x_{N-L+1} \end{bmatrix}_{L\times N}$, substituting Eqs. (3) and (4) into Eq. (5) gives:

$$\boldsymbol{f} = \frac{\sum_{j=1}^{N} y_j^2}{\sum_{j=1}^{N} y_j^4} \left(\boldsymbol{X}_0 \boldsymbol{X}_0^T\right)^{-1} \boldsymbol{X}_0 \left[y_1^3 y_2^3 \cdots y_N^3\right]^T \tag{6}$$

MED specific flow paths are as follows:

(1) Initialize $\boldsymbol{f}^{(0)} = (0, 1, 0, \ldots, 0)^T$ meanwhile input the raw signal $\boldsymbol{x}$ to get $\boldsymbol{X}_0^T$.

(2) Set filter length $L$, the maximum count of iterations $m_{\max}$, and convergence error $\varsigma$.

(3) According to Eq. (5), calculating $y^m(j)$ by substituting $\boldsymbol{X}_0^T$ and filter coefficient $f^m(l)$, then get the $f^{m+1}(l)$ by Eq. (6).

(4) According to Eq. (3), calculate the error $\Delta E = \left|O_4(f^{(m+1)}) - O_4(f^{(m)})\right|$.

(5) If $m < m_{\max}$ and $\Delta E < \varsigma$, continue cyclic iteration from **step. (3)**, otherwise, output the final filter coefficient $f^{end}(l)$ and $y^{end}(j)$ is outputted according to Eq. (5).

### 2.2. The effect of filter length on enhancing the periodic impulses

In order to show the importance of filter length $L$ in MED more intuitively, a simulation signal as shown in Fig. 2 is established:

$$x(t) = s(t) + n(t) + h(t) \tag{7}$$

Fig. 2(a) shows the fault impulses whose fault-sampling intervals are 30 points. $n(t)$ is the white Gaussian noise and mixed with the fault signal as shown in Fig. 2(b) and the energy ratio of impulses to noise is 0.22. Fig. 2(c) shows the observation signal $x(t)$, in which the harmonic component $h(t) = 0.1\sin(2\pi f_1 t) + 0.2\sin(2\pi f_2 t) + \sin(2\pi f_3 t)$ , $f_1 = 4f_2 = 2f_3 = 1/15$. The length of the signal is 2000.

The observation signal is filtered by MED at the filter length $L = 150$ and 151, respectively. The results are shown in Fig. 3. When $L = 150$, the output signal is a single random pulse, which is not we want because we expect to recover a series of periodic fault features from the weak signal for the detection of rotating machinery, so it is useless. However, in the case of $L = 151$, the periodic impulses are very clear. It is remarkable that the difference between the two filter length values is only 1, but their outputs are entirely different. This phenomenon shows that the filter length has a great influence on the output of MED. Choosing a suitable filter length is a key step in the MED method. In order to avoid the occurrence of single pulse maximization, it is necessary to study the method of choosing filter length accurately, because the experience may bring the wrong result.

## 3. Selection of the optimal filter length

To give full play to the potential of MED to enhance the weak periodic impulses, it is necessary to establish the objective

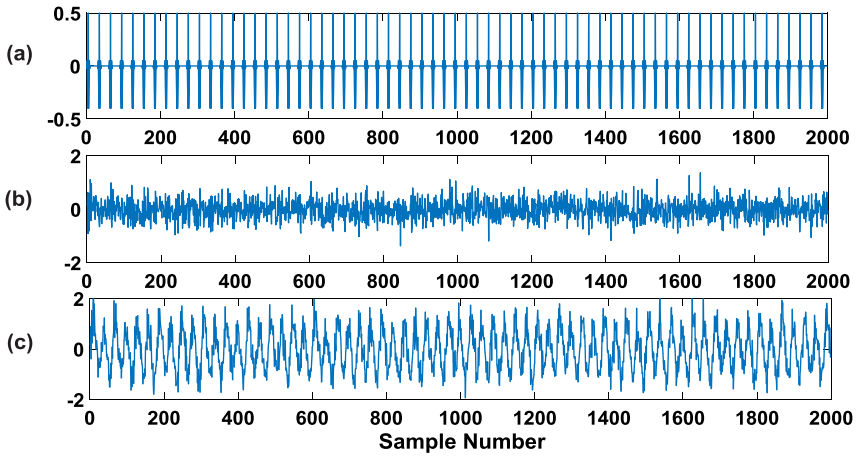


**Fig. 2.** The simulated fault signals. (a) Fault impulses; (b) Noise with fault impulse; (c) Observation signal.

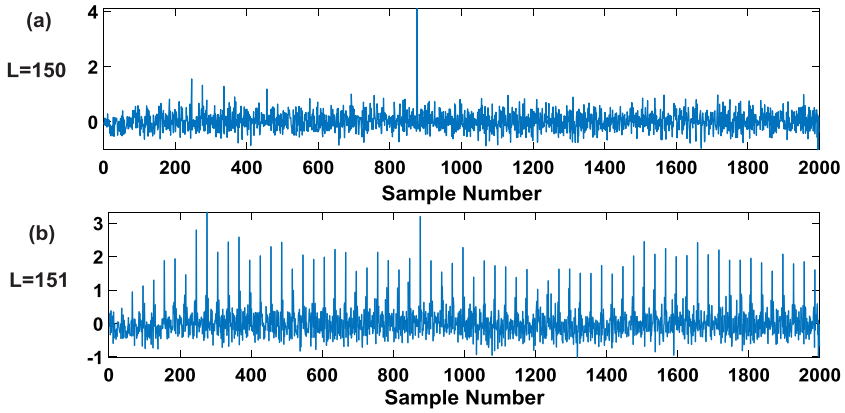


**Fig. 3.** The filtered signals using MED with different filter lengths. (a) $L = 150$; (b) $L = 151$.

function to measure the periodicity of the output signal. In this paper, autocorrelation function and signal energy are used to solve the problem of selecting the optimal filter length.

### 3.1. Autocorrelation analysis

Autocorrelation analysis reflects the similarity of the signal itself at different moments or phases, which is an effective method to determine whether the signal has periodicity. Suppose $s(t)$ is a sinusoidal periodic signal to be measured. $n(t)$ is Gaussian white noise. The observation signal is:

$$x(t) = s(t) + n(t) = A\sin(\omega_0 t + \phi) + n(t) \tag{8}$$

Doing autocorrelation analysis on $x(t)$ gives that:

$$R_x(\tau) = E[x(t)\,x(t-\tau)] = R_s(\tau) + R_n(\tau) + R_{sn}(\tau) + R_{ns}(\tau) \tag{9}$$

In fact, $n(t)$ and $s(t)$ are independent of each other, so $R_{sn}(\tau) = R_{ns}(\tau) = 0$, that is:

$$R_x(\tau) = R_s(\tau) + R_n(\tau) = \lim_{T\to\infty}\frac{1}{2T}\int_{-T}^{T}[s(t)\,s(t-\tau)]\,dt + R_n(\tau) = \frac{A^2}{2}\cos(\omega_0\tau) + R_n(\tau) \tag{10}$$

where $A$ is the amplitude, $\omega_0$ is the angular frequency, $\phi$ is the initial phase. Since $n(t)$ is noise, $R_n(\tau)$ is concentrated around$\tau = 0$ as shown in Fig. 4. $R_s(\tau)$ is a signal with the same $\omega_0$ as $s(t)$ from Eq. (9). When $\tau$ becomes larger, $R_x(\tau)$ only reflects $R_s(\tau)$, so the amplitude and frequency of $s(t)$ can be obtained by$R_x(\tau)$ as shown in Fig. 5.

### 3.2. Establishment of the objective function

The limitation of MED is that iterative calculation can only be performed under a specific filter length, so the outputs of different filter lengths are different. The main purpose of the objective function is to establish an index to measure the periodicity of the output signal at different filter lengths.

Assuming that given a priori filter length $L$, the output signal is $\boldsymbol{y}_L$, then the remaining components of the raw signal are expressed as:

$$\boldsymbol{S}_L = \boldsymbol{x}_N - \boldsymbol{y}_L \tag{11}$$

$\boldsymbol{x}_N$ is the raw signal. The objective function can be defined as:

$$L_\mu = \frac{\sum_{n=1}^{N} {R_{\boldsymbol{y}_L}}^2(n)}{\sum_{n=1}^{N} {R_{\boldsymbol{S}_L}}^2(n)} \tag{12}$$

where $N$ is the length of data, $R_{\boldsymbol{y}_L}(\cdot)$ represents the autocorrelation of the output signal, $R_{\boldsymbol{S}_L}(\cdot)$ represents the autocorrelation of the residual components. When the output signal approaches the periodic impulse, its autocorrelation is also approximately a periodic signal. At this moment, MED maximizes the kurtosis of the continuous weak impulses, which also suppresses the system harmonics and noise. Therefore, the energy ratio of the output signal to the residual signal will be a larger value. Conversely, when the output signal is a single pulse, except for an impact characteristic of the larger amplitude at a certain time in the time domain waveform, most of the residual part is the noise, so in its autocorrelation waveform, the amplitude mainly appears at 0 moments. The amplitudes at the other moments are very small

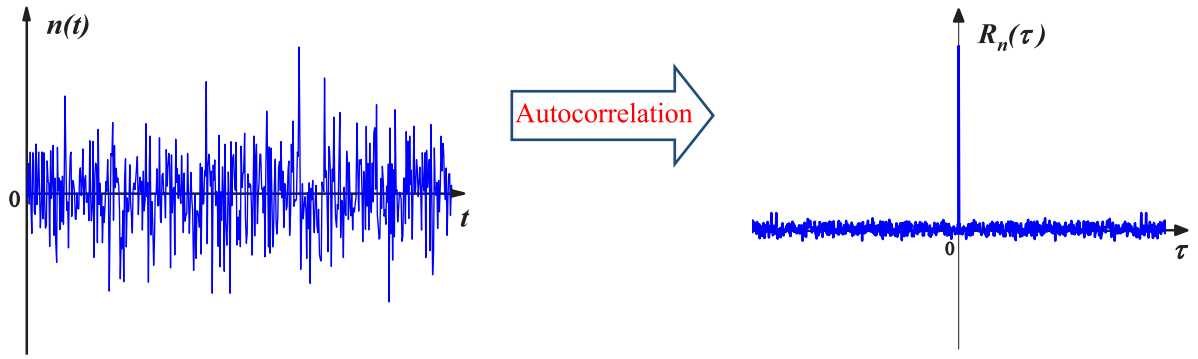


**Fig. 4.** The autocorrelation analysis of Gaussian white noise.

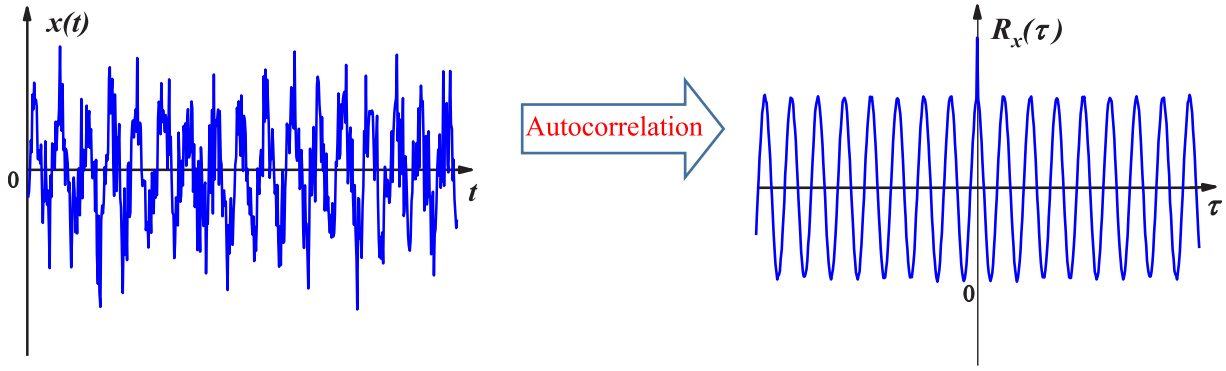


**Fig. 5.** The autocorrelation analysis of periodic signal with noise.

and close to 0. Thus, the energy ratio will be a smaller value. The magnitude of $L_\mu$ can be used as a basis for judging whether the output result is a periodic pulse. To eliminate interference, remove the amplitude of autocorrelation at 0 moments. There is an example to illustrate the superiority of the $L_\mu$ index. For the simulation signal of Eq. (7), Fig. 6 plots the kurtosis and $L_\mu$ of the MED-filtered outputs from $L = 2$ to $L = 500$. It can be seen from Fig. 6(a) that as the filter length increases, the value of kurtosis also increases, which is consistent with the conclusion given in Ref. [15]. This result is not difficult to understand because the objective function in MED aims to maximize the kurtosis of the signal. Kurtosis is a good indicator of impact characteristics. However, the variation of kurtosis is not related to whether the output signal is the continuous impulses so the kurtosis is not the bigger the better in MED. It can easily raise a single large pulse to satisfy the case of high kurtosis of the whole signal. Therefore, to avoid such a situation, it is particularly important to obtain the periodic impact signal when kurtosis value is as large as possible. Fig. 6(b) plots the variation of $L_\mu$ under different filter lengths. The overall trend of $L_\mu$ is to go up first then down to stabilize. When $L = 150$ and $L = 151$, the outputs are hugely different as shown in Fig. 3. Fig. 7 shows the outputs at $L = 50$, 167 and 168, respectively. It can be seen from the results that the larger the $L_\mu$ is, the better the filtered effect and the stronger the periodic impact feature is. After $L = 168$, $L_\mu$ tends to decline steadily, which means that the outputs will be the single pulse and MED will lose the ability to enhance the periodic weak signal. So $L_\mu$ can be regarded as the objective function to optimize the length of the MED filter.

### 3.3. Global optimization of genetic algorithms

Genetic algorithms (GA) is a kind of self-organizing and adaptive artificial intelligence technology that simulates the biological evolution process and mechanism of nature to solve extreme value problems. It was proposed by Holland [22] and has a wide range of applications [23–25]. In the field of fault diagnosis, GA also has excellent results [26,27]. In MED, the filter length can be any integer less than the raw signal length. Therefore, in this paper, the main function of GA is to search the maximum value of $L_\mu$ under the global filter length.

GA mainly includes the following contents: defining the population, coding individuals, calculating individual fitness (objective function), selection (heredity), crossover, and mutation. The main steps of the genetic algorithm are: (1) Randomly generate $M$ individuals as an initial population. (2) Calculate the fitness of each individual in the population. (3) Selection operation, the purpose is to select some excellent individuals to pass them on to the next generation. (4) Each individual in the population is randomly matched to exchange part of their chromosomes with a certain probability, and each individual has a certain probability of mutation. (5) After multiple evolutions (iterations), the best individuals are finally preserved.

This study uses the binary method to encode the individuals of the populations. The objective function is in Eq. (11). "Roulette" algorithm is used for the selection of the population, that is:

$$p(x_i) = \frac{f(x_i)}{\sum_{j=1}^{N} f(x_j)} \tag{13}$$

The probability of each individual $x_i$ being selected is$p(x_i)$. $f(x_i)$ is the fitness calculated by the objective function. The cumulative probability of each individual is:

$$Q(x_i) = \sum_{k=1}^{i} p(x_k) \tag{14}$$

Randomly generated$r \in [0, 1]$, if $Q(x_i) > r$, select $x_i$. The probabilities of crossover and mutation are 0.6 and 0.001 respectively [28].

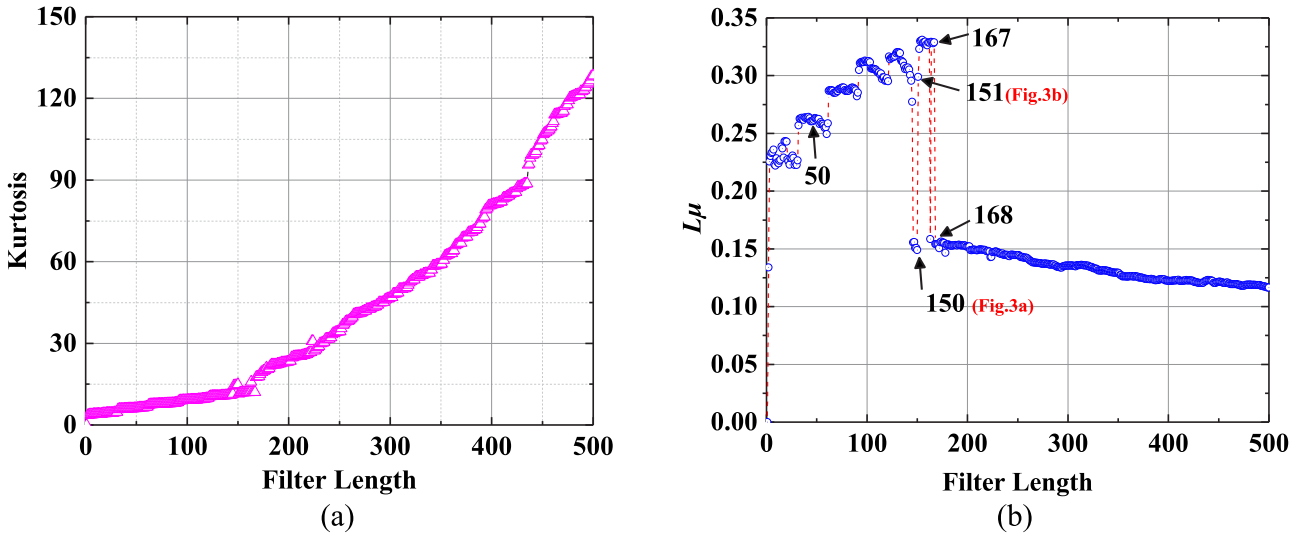


**Fig. 6.** (a) Kurtosis and (b) $L_\mu$ of the outputs at different filter lengths.

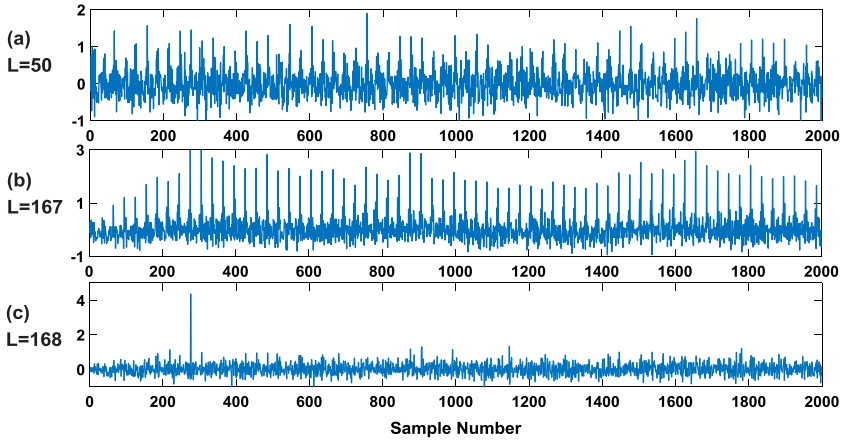


**Fig. 7.** The outputs at different filter lengths. (a) $L = 50$; (b) $L = 167$; (c) $L = 168$.

Fig. 8 discusses the effect of populations on search results. The population sizes are 25, 50, 75, and 100, respectively. The number of iterations is 100. The results in Fig. 8(a) illustrates that the mean fitness is not optimal in a small population. As the population increases, the mean fitness will gradually approach its maximum. The optimal filter length and mean fitness is $L = 162$, $L_\mu = 0.328$, which is consistent with the result in Fig. 6(b). There is a logarithmic trend between population growth and fitness function in Fig. 8(b), which indicates that when the population reaches a certain degree, the mean fitness will reach a mature state. Fig. 9 shows the outputs under the optimal search of four populations. From the corresponding filtering effects, even if the small population does not reach the maximum value of the fitness $L_\mu$, some better periodic impulses can be obtained. This is because GA is always looking for the "optimal" solution in a limited population, so there is no need to worry about the situation where the fitness $L_\mu$ is very low and the filtered result becomes a single impulse. So, this is the reason why this paper chooses the GA method for global optimization. In order to achieve better results, both the population size and the number of iterations are set to 100 in this study.

According to the above analysis, the specific flows of the MED optimal filter length selection method proposed in this paper are shown in Fig. 10, as follow steps:

(1) Set the parameters of GA and randomly generate populations (filter lengths) and binary encode them. The encoding length depends on the length of the raw signal.

(2) Take $L_\mu$ as the objective function to calculate the fitness of each individual. Form new populations after crossover and mutation.

(3) After $N$ iterations or reaching the iteration error, output the best individual to get the filter length.

## 4. Application in fault detection of rolling bearing

When the bearing raceway is damaged, such as peeling, cracking, pitting, etc. impact vibration is usually generated when a rolling element passes, resulting in a series of periodic or quasi-periodic impacts. These impulses are mixed with system noise. Due to the limitations of the structure transmission path and the sensor position, in the collected signal, the impact characteristics will be very weak. To fully illustrate the advantage of the proposed method, this section is verified by rolling bearing failure experiments in two sets of situations. The first one is the run-to-failure test of rolling bearing provided by the IMS center, aiming at verifying the diagnostic ability of the proposed method under the strong background noise interference in the early stage of fault initiation. The second is the fault experiment of rolling bearing using an aero-engine rotor experimental rig with casing.

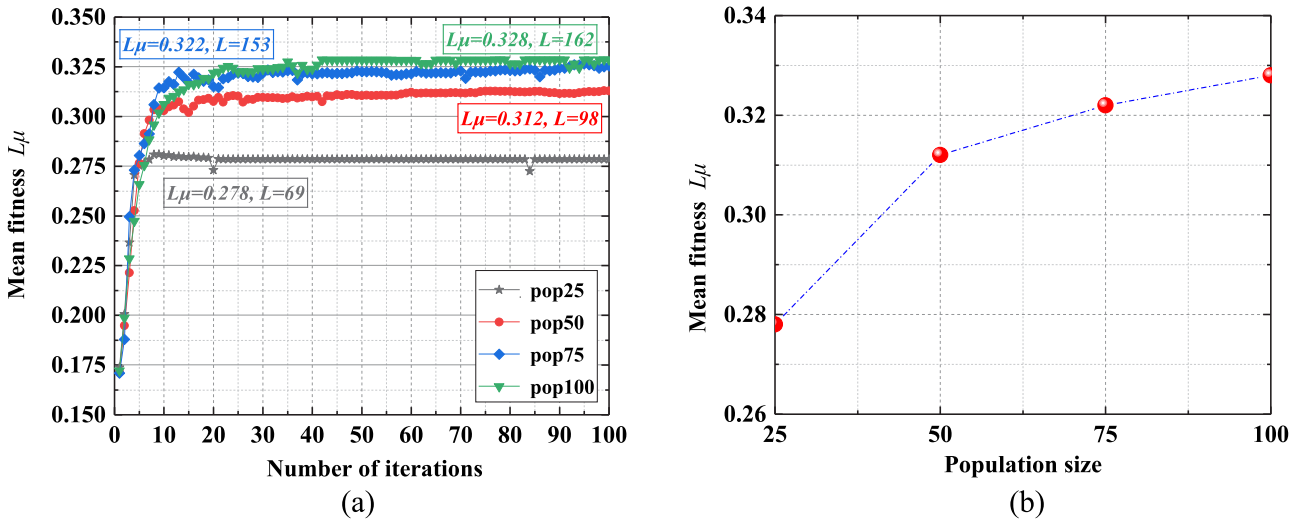


**Fig. 8.** The effect of populations on search results. (a) Optimal filter length under different populations (iterations 100). (b) Mean fitness in different populations.

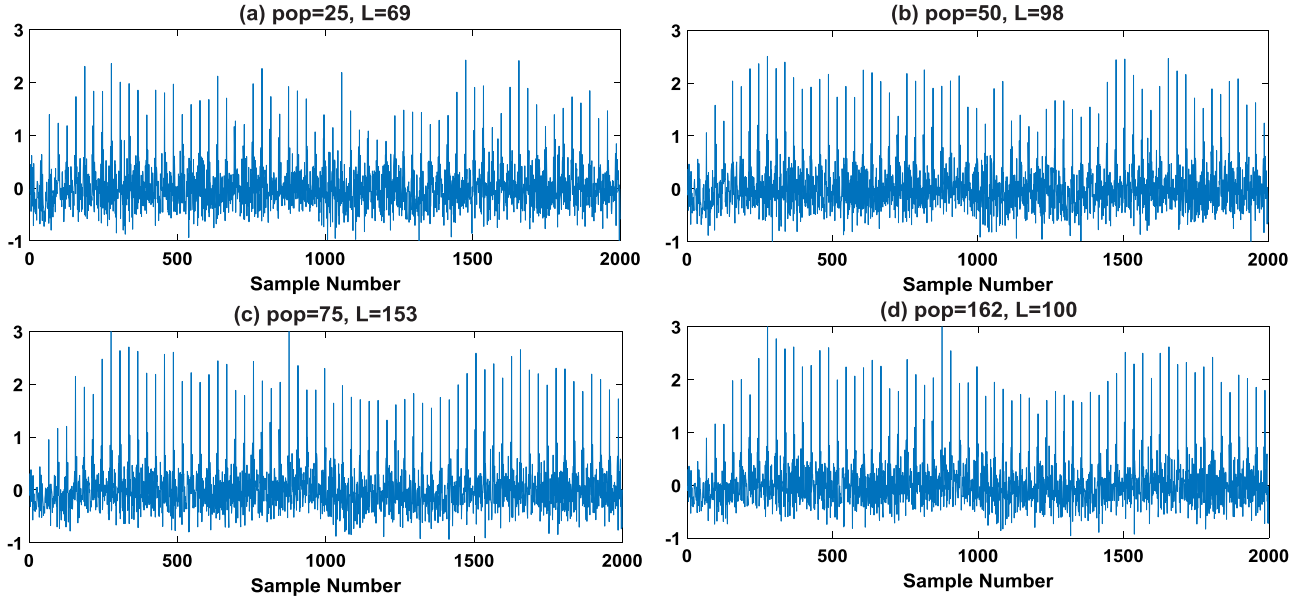


**Fig. 9.** The outputs of different populations. (a) pop = 25, $L = 69$; (b) pop = 50, $L = 98$; (c) pop = 75, $L = 153$; (d) pop = 100, $L = 162$.

Detecting the casing signal to simulate the attenuation of the fault characteristics by the transmission path, the superiority of the proposed method is verified.

### 4.1. Detection of run-to-failure test

The test data are generated by the IMS center (www.imscenter.net). The test rig in Fig. 11 consists of four bearings mounted on the shaft, which is connected to the motor by a friction belt. The bearings are Rexnord ZA-2115, whose dimensions are given in Table 1. The radial load on the bearing was 6000 lps and the rotation speed was 2000 rpm. PCB 353b33 ICP acceleration sensors were placed on each bearing housing with a sampling frequency of 20.48 kHz. The number of sampling points for each record was 20 480 and the sampling interval was 10 min. More details can be found in Ref. [29].

After 984 records were collected, the outer race of No. 1 bearing failed. The root means square (RMS) value of No. 1 bearing is shown in Fig. 12. Set the failure threshold as $\lambda = \mu + 3\sigma$. $\mu$ and $\sigma$ are the mean and variance of RMS of the first 200 normal records respectively. At 533 record, the RMS value is outside the threshold range indicating that the bearing condition has changed. Therefore, the vibration signal at 533 record is selected as the sample of detection and its time domain waveform is shown in Fig. 13. In the research of Ref. [18], 533 record is also taken as the sign of early failure. However, when the MED+SK (Spectral kurtosis) +SES (Square envelope spectrum) method was applied to detect 533 record, no-fault characteristic frequency of the bearing was found in Fig. 14. The authors in Ref. [18] set the filter length of the MED as 1000 based on experience. Fig. 15(a) plots the output of MED at the filter length of 1000. It can be seen that a single large pulse has appeared at this time, which indicates that the MED has lost the ability to enhance the periodic impact features. For SK method, it is very sensitive to kurtosis.

**Table 1**
Rexnord ZA-2115 bearing dimensions (unit: mm).

| Type | Pitch diameter | Diameter of roller | Roller number | Contact angle |
|---|---|---|---|---|
| ZA-2115 | 71.5 | 8.4 | 16 | 15.17° |

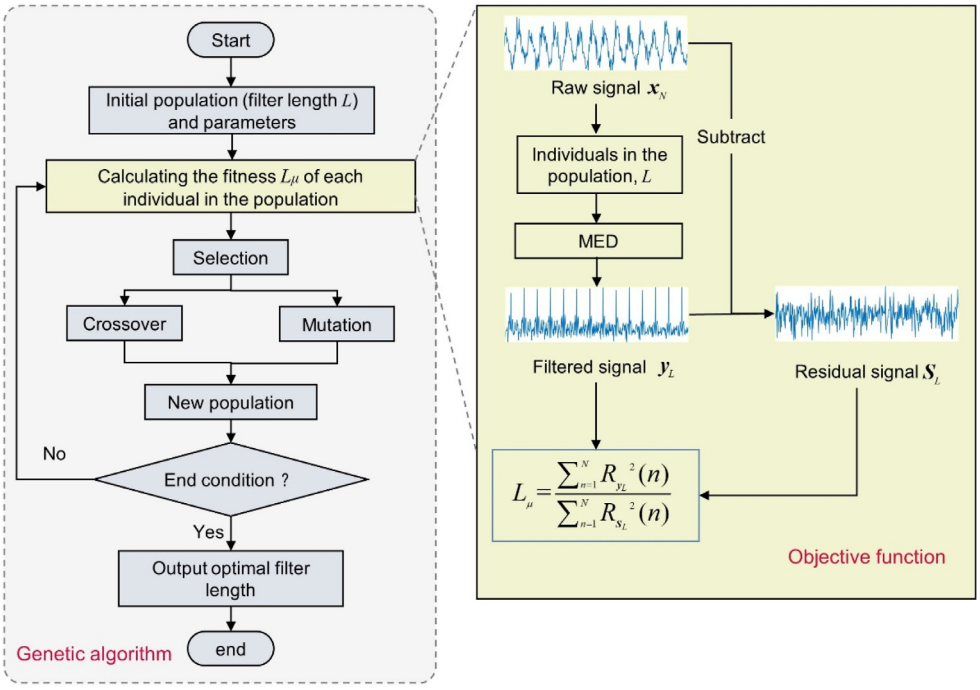


**Fig. 10.** The process of selecting the optimal filter length.

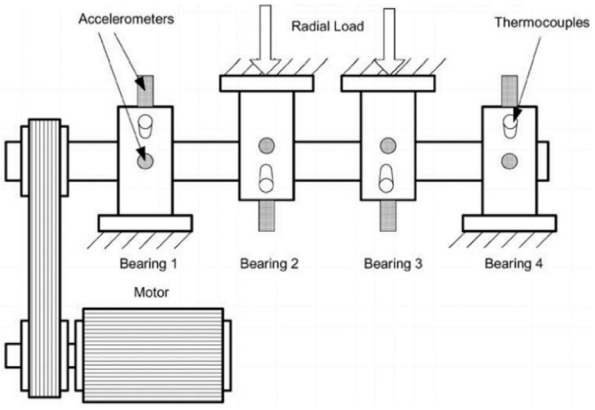


**Fig. 11.** Run-to-failure test rig.

Random single large pulse will interfere with its detection effect. Consequently, its detection result is bound to fail. Fig. 15(b) shows the envelope spectrum of Fig. 15(a) which is filled with abundant noise and no conspicuous BPFO (236 Hz) in the spectrum.

According to the above analysis, the early failure characteristics of the bearing cannot be detected at 1000 filter length. Next, using the proposed method in this paper to detect the 533 record. The optimal filter length is $L = 61$, $L_\mu = 0.452$ by GA global optimization which is shown in Fig. 16(a). Fig. 16(b) is the result of the objective function $L_\mu$ in the range of 2–2000 filter length. It can be seen that the value of $L_\mu$ is 0.184 when the filter length is 1000. The small value indicates that the MED has failed. The output of MED with $L = 61$ is in Fig. 17. Although there are still noises in the time domain waveform, the useful information remains in the signal. Moreover, in its envelope, we can see the obvious BPFO and its harmonic components. In addition, the method of MED+SK+SES is used to detect 533 record at $L = 61$. From the result of Fig. 18, the BPFO is also conspicuous. Consequently, MED can extract the early fault features of No. 1 bearing in the case of optimal filter length. Conversely, inappropriate filter length will lead to an erroneous result.

### 4.2. Detection of weak fault casing signal

In some cases, the vibration sensors will not be installed close to the bearings because of the complex internal structure, such as in aero-engine, so they will be placed on the casing. Because of the transmission path and other structural noise, the bearings' fault information will become even weaker after being transmitted to the casing, which brings great challenges to the detection. In order to verify the contribution of the proposed method in eliminating the effect of the transmission path, an aero-engine rotor test rig with the casing is built to simulate the situation far away from the bearing vibration source.

The aero-engine rotor test rig is very close to a real aero-engine as shown in Fig. 19. Its typical features are as follows: (1) It has a multi-segment casing with a ratio of 1:3 to the real engine. (2) The internal structures are simplified. Two disks with blades represent the compressor disk and the turbine disk respectively and two bearings are installed between them. The compressor end is roller bearing and the turbine end is ball bearing. (3) The support stiffness can be adjusted by changing the elastic support position. (4) The rotor without the combustion chamber structure is driven by the motor.

The faulty ball bearings whose type is HRB 6206 in Fig. 20 were installed at the turbo end respectively. The width and depth of the wire-electrode cutting cracks on the outer and inner races are both 2 mm. The crack on the ball is 1 mm width and 2 mm depth. Table 2 gives the dimensions of the bearings. Two B&K4805 ICP acceleration sensors were placed on the vertical and horizontal directions of the casing respectively and one was attached to the bearing housing, as shown in Fig. 21. Fig. 22 shows the vibration transmission path from the bearing housing to the casing, that is: ball bearing — squirrel cage — elastic support — turbo stator — casing (sensors). The distance is longer than the engine radius (180 mm). The sampling rate was 10.24 kHz and each data contain 8192 points. The bearing housing signal and casing signal

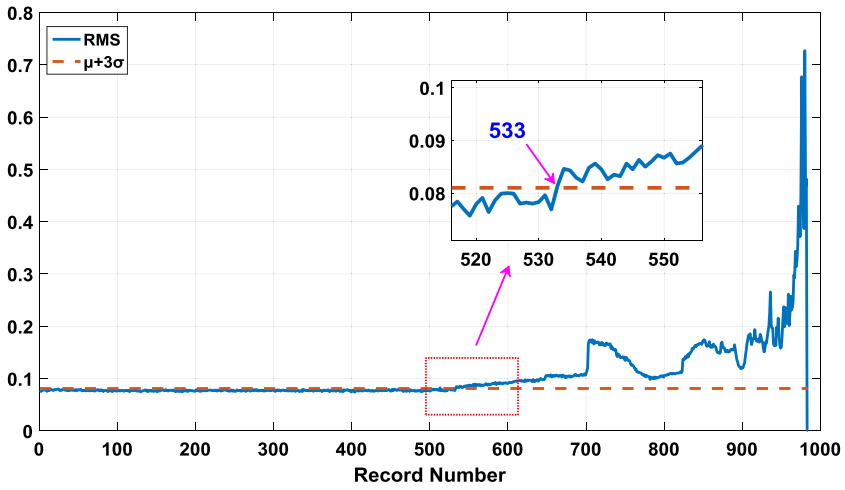


**Fig. 12.** The RMS of bearing No.1.

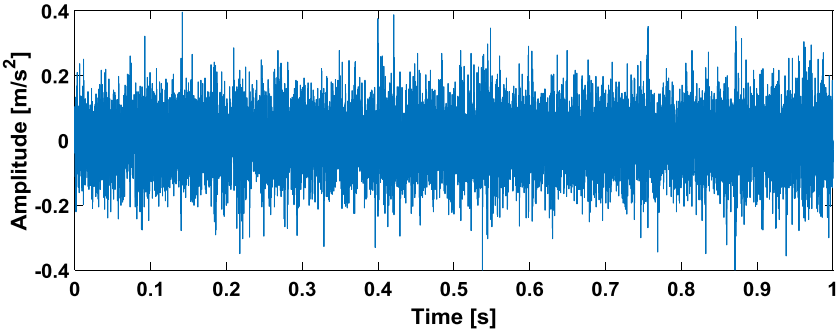


**Fig. 13.** The time domain waveform of 533 record.

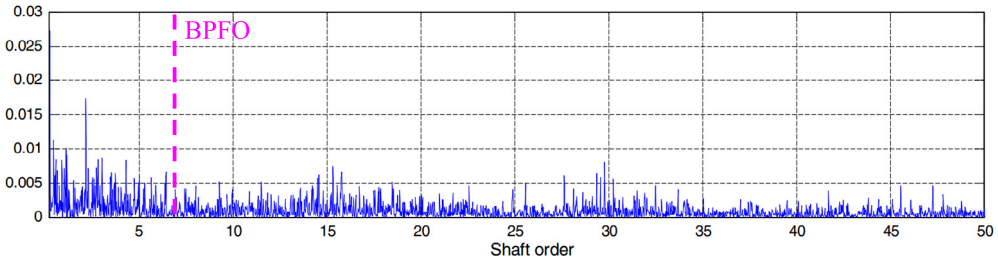


**Fig. 14.** The detection result of MED+SK+SES in Ref. [18] (MED filter length is 1000).

**Table 2**
6206 ball bearing dimensions (unit: mm).

| Type | Pitch diameter | Diameter of ball | Ball number | Contact angle |
|---|---|---|---|---|
| 6206 | 46 | 9.5 | 9 | 0 |

were collected for detection respectively. The rotation speeds were 1500 rpm.

For the outer race fault bearing, Fig. 23 draws the time domain waveforms and envelope spectra of the bearing housing signal and the casing vertical measuring point signal. The fault feature of bearing housing is highlighted. In the time domain waveform, Fig. 23(a), it has clear periodic impulses and large amplitude. In the envelope spectrum, Fig. 23(c), BPFO (92 Hz) and its harmonics are obvious. However, for the casing signal, the impulses are masked by a large amount of noise in Fig. 23(b). The amplitude decays nearly 10 multiples. The BPFOs in the Fig. 23(d) are covered by other frequencies. Thus, it is difficult to directly detect the fault information of the casing signal that far away from the vibration source.

In order to overcome the above problem, the proposed method is used to detect the casing signal. After GA global search, the result of the optimal filter length is $L = 157$, $L_\mu = 0.362$ as shown in Fig. 24(a). Fig. 24(b) depicts the variation of $L_\mu$ under the 2–500 filter length where the effective filter lengths are limited and the values of $L_\mu$ are less than 0.1 at most filter lengths. To illustrate the advantage of the proposed method more visually, the optimal filter length ($L = 157$) and the low $L_\mu$ value filter length ($L = 154$) are selected for comparison as shown in Fig. 25. Fig. 25(a) is the time domain waveform after optimal filter length filtered and Fig. 25(b) is its envelope spectrum. From the results, the periodic fault impulses have been fully enhanced. The BPFO and its harmonics are conspicuous. Compared with Fig. 23(c), the harmonics of 3BPFO and 4BPFO are more prominent. However, in the case of $L = 154$, the results are totally different. A single sharp impulse is in Fig. 25(c) and there are no fault features in

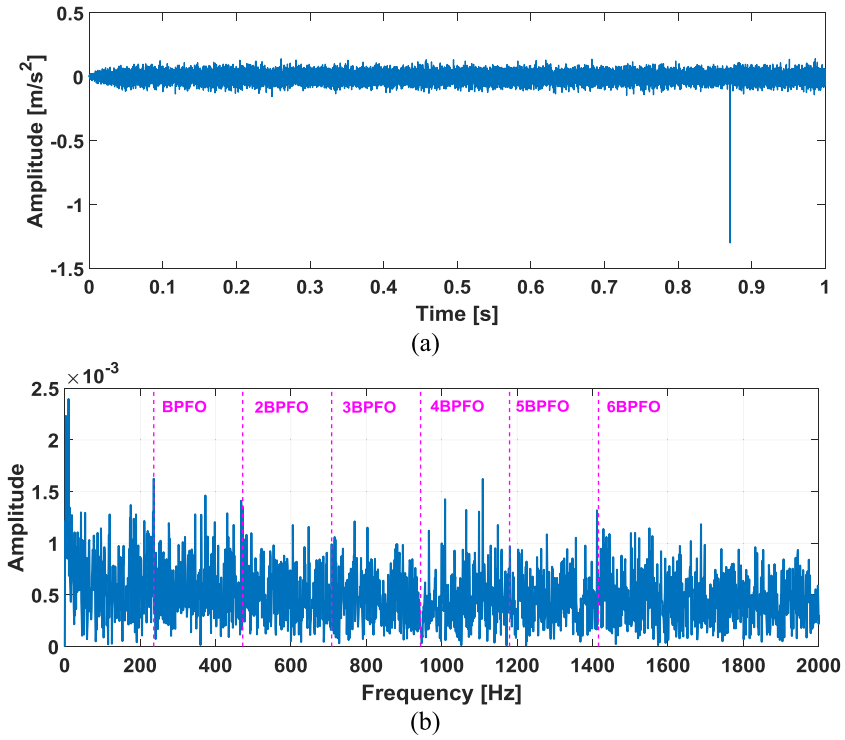


**Fig. 15.** The output result of 533 record at filter length 1000. (a) Time domain waveform; (b) Envelope spectrum of (a).

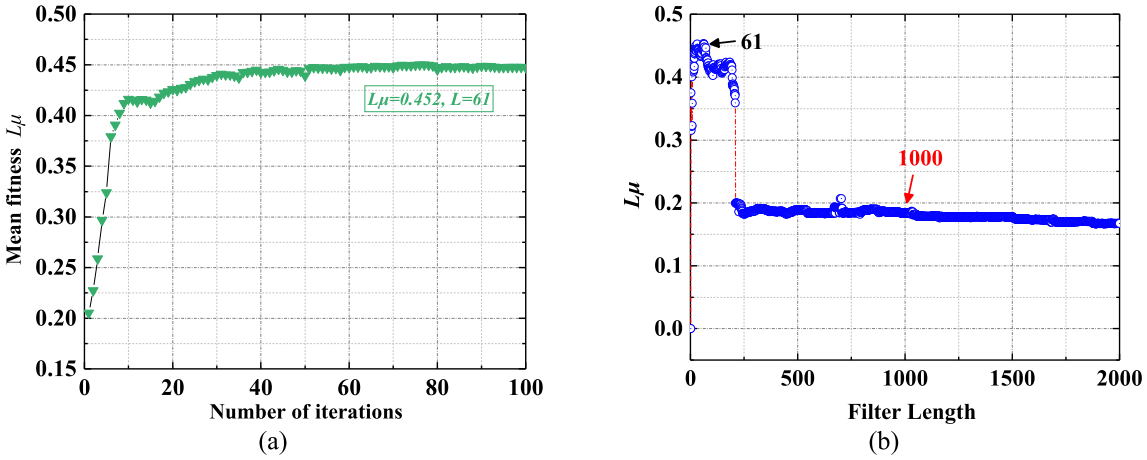


**Fig. 16.** The selection of optimal filter length for 533 record. (a) Results of GA optimization; (b) The value of $L_\mu$.

its envelope, which is not the result we expected. Therefore, a suitable filter length is vital.

Similarly, for the inner race fault bearing, the horizontal measuring point signal of the casing is selected for analysis. Fig. 26 shows the comparison between the bearing housing signal and the casing signal. In Fig. 26(a) the fault periodic impulses are obvious and their amplitudes are large. In its corresponding envelope spectrum Fig. 26(c), the ball pass frequency on inner race (BPFI = 135 Hz) and its harmonics can be seen clearly, and there is a phenomenon of rotation modulation (fr = 25 Hz). However, in Fig. 26(b), the periodic impulses are submerged by noise and the amplitude has decreased nearly 20 multiples. In the envelope spectrum, as shown in Fig. 26(d), BPFIs are not recognized. These above results indicate once again that the fault features in the casing signal are very weak.

We use the method proposed in this paper to diagnose the casing signal of inner race fault. The results of the optimal filter length after GA optimization are shown in Fig. 27. The optimal filter length is $L = 100$, $L_\mu = 0.236$. At this filter length, the output of the inner race fault is plotted in Fig. 28(a) where the continuous impulses in the casing signal are more obvious compared with Fig. 26(b). In the envelope spectrum, Fig. 28(b), The BPFI, 2BPFI, and 3BPFI are all conspicuous and the rotation modulation exists. However, the situations are quite different when $L = 101$. MED cannot recover the periodic impulses. The time domain waveform appears as a large single impact due to improper filter length in Fig. 28(c). The BPFI and its harmonics are inapparent.

As for the ball fault bearing. Fig. 29 depicts the detection results of the bearing housing signal and the casing signal. The situation is the same as the outer race fault and inner race fault. The fault feature of bearing housing is prominent but the casing signal has no fault information. Note that in Fig. 29(c) the even harmonics of ball spin frequency (BSF) are dominant in particular

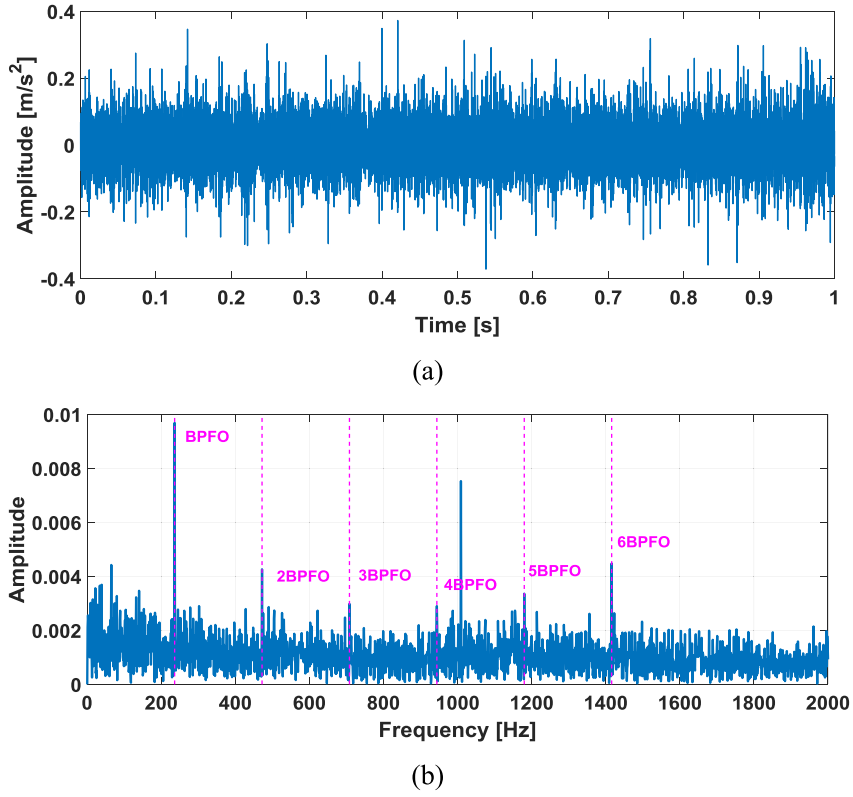


**Fig. 17.** The output result of 533 record at optimal filter length. (a) Time domain waveform; (b) Envelope of (a).

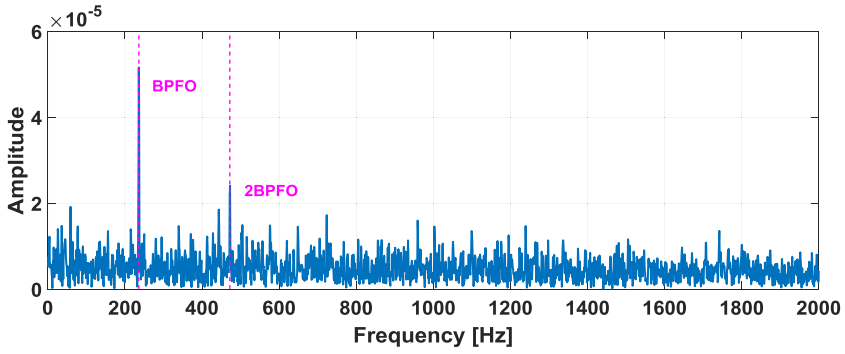


**Fig. 18.** The results of MED+SK +SES at optimal filter length.

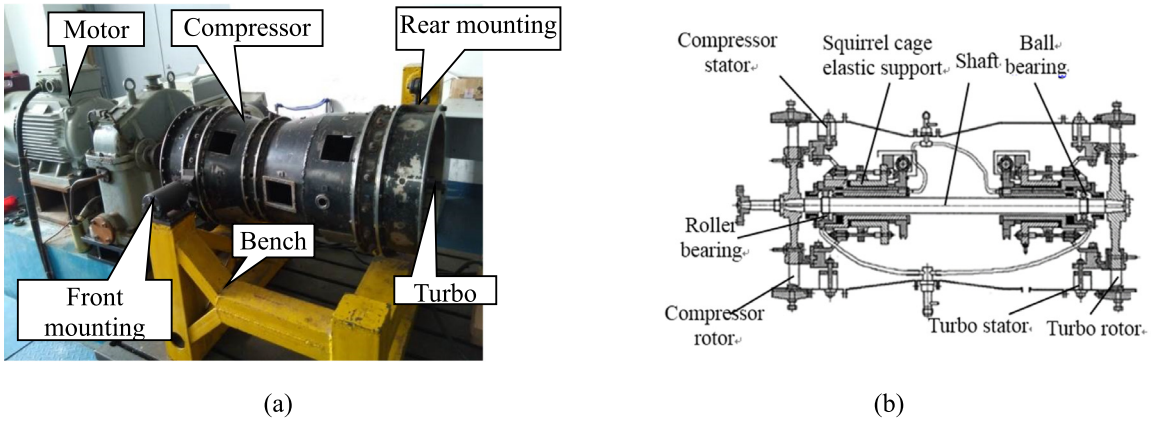


**Fig. 19.** Aero-engine rotor test rig. (a) Side view (b) Sectional view.

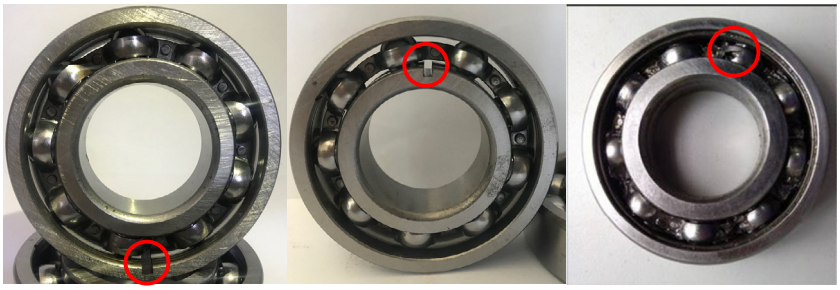

**Fig. 20.** 6206 ball bearing of outer race fault, inner race fault and ball fault.

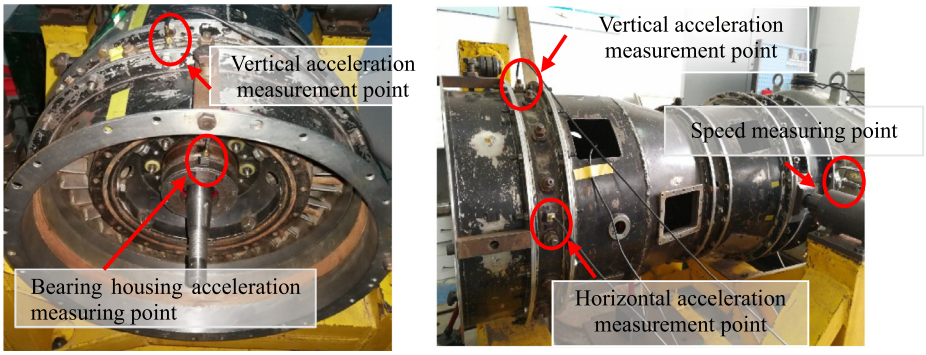


**Fig. 21.** The locations of bearing housing measuring point and casing measuring points.

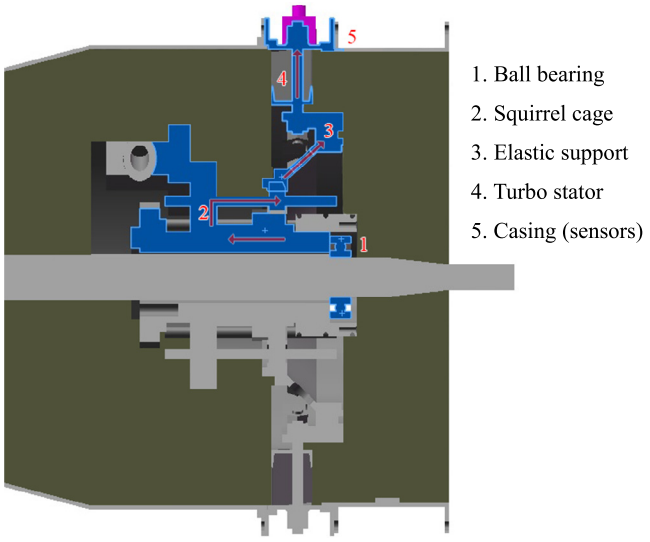


**Fig. 22.** The vibration transmission path from bearing housing to casing (turbo end section).

in the envelope spectrum [1]. The 2BSF is 115 Hz with the cage frequency modulation (second harmonic, fc = 20 Hz).

Fig. 30 plots the results of optimal filter length after GA optimization. The best fitness value of $L_\mu$ is 0.176 and the optimal filter length is 46. Fig. 31(a) is the time domain waveform after MED filtered at optimal filter length. Its envelope is in Fig. 31(b). From the results, the impulses in the casing signal have been enhanced and 2BSF can be found in the envelope spectrum. However, the cage modulation frequency cannot be seen obviously. Because the ball has great randomness and slip in the process of rotation, and the ball crack is relatively small, which makes its impacts less intense than the outer race fault and inner race fault. When the filter length is 76, there is no fault information in the envelope, which indicates that MED has lost the detection ability.

According to the detection results of casing signals, it is clearly stated that the selection of the length of the MED filter is extremely important to the output result. Appropriate filter length can fully enhance the continuous periodic impulse characteristics, while wrong filter length will make MED lose its ability to recover the impacts in weak signals, which will bring adverse consequences for the diagnosis of bearing fault. The proposed method in this paper can avoid this problem well.

## 5. Comparison with other MED-based methods

At present, there are two main ways to improve MED: optimizing the filter coefficients [13,14] and transforming kurtosis into other objective functions [7–12]. In this section, to further illustrate the advantages of the proposed method, two advanced detection methods, PSO-MED and MCKD method were selected for comparative analysis.

### 5.1. Comparison with PSO-MED

Cheng [13] proposed an improved MED method based on particle swarm optimization (named PSO-MED). In this method, the filter coefficients are transformed into generalized spherical coordinates, and the standard PSO is used to calculate the optimal solution. It shows that the PSO-MED outperformed MED when the signal-to-noise ratio is low. For the sake of fairness, the parameters of PSO-MED in this article are the same as those in Ref. [13]. Besides, PSO-MED needs to set the filter length in advance, so the optimal filter lengths proposed in this paper are selected to detect the 533 record and the casing signals. The MATLAB codes of PSO-MED can be downloaded from the Mendeley data [30].

Fig. 32 shows the envelope spectrum of 533 record after PSO-MED filtered. We can see the BPFO and its harmonics are apparent, which indicates that PSO-MED has good performance in the detection of 533 record. However, the results are not ideal

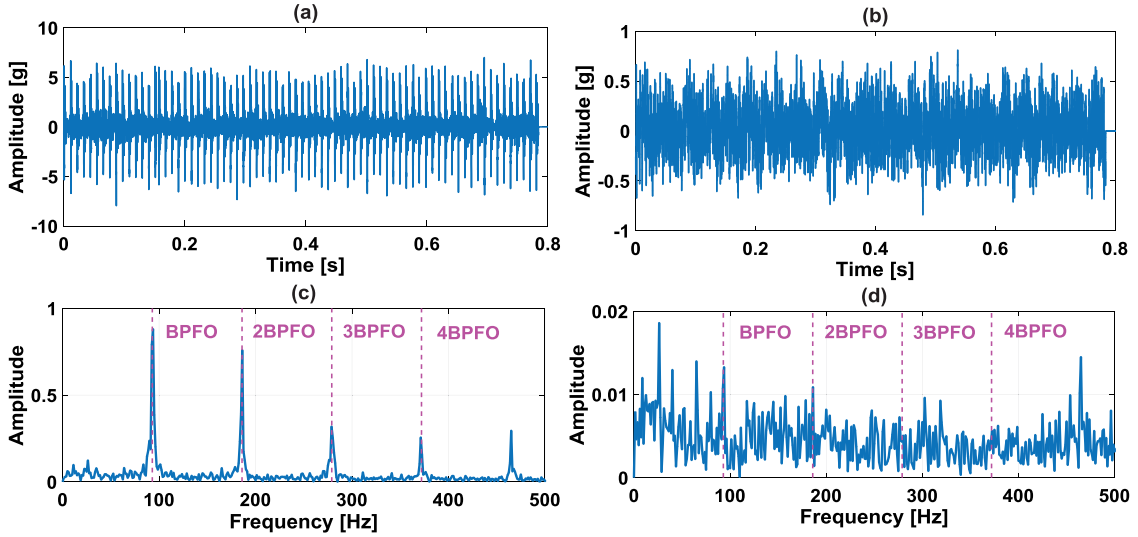


**Fig. 23.** The time domain waveforms and envelope spectra of the outer race fault. (a) Bearing housing; (b) Casing vertical measuring point signal; (c) Envelope spectrum of (a); (d) Envelope spectrum of (b).

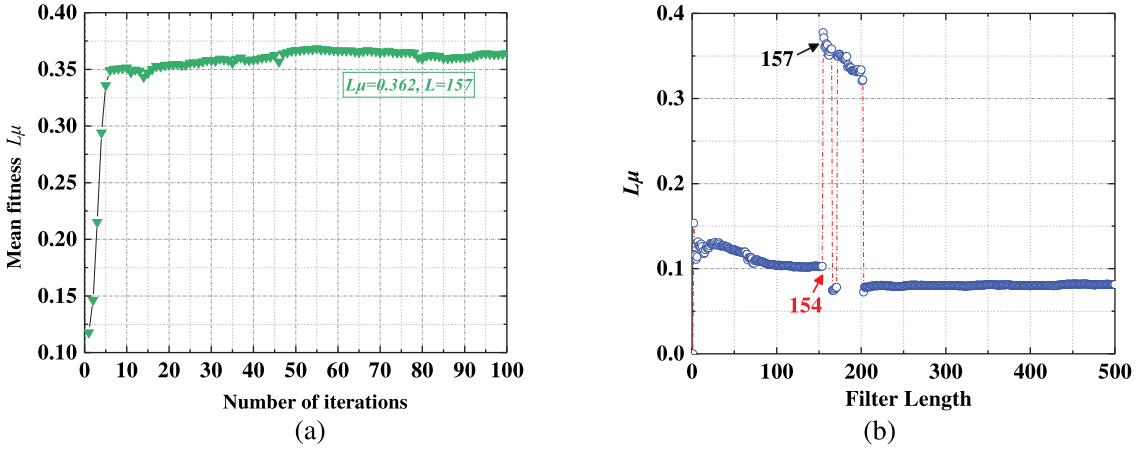


**Fig. 24.** The selection of optimal filter length for casing signal of the outer race fault. (a) Results of GA optimization; (b) The value of $L_\mu$.

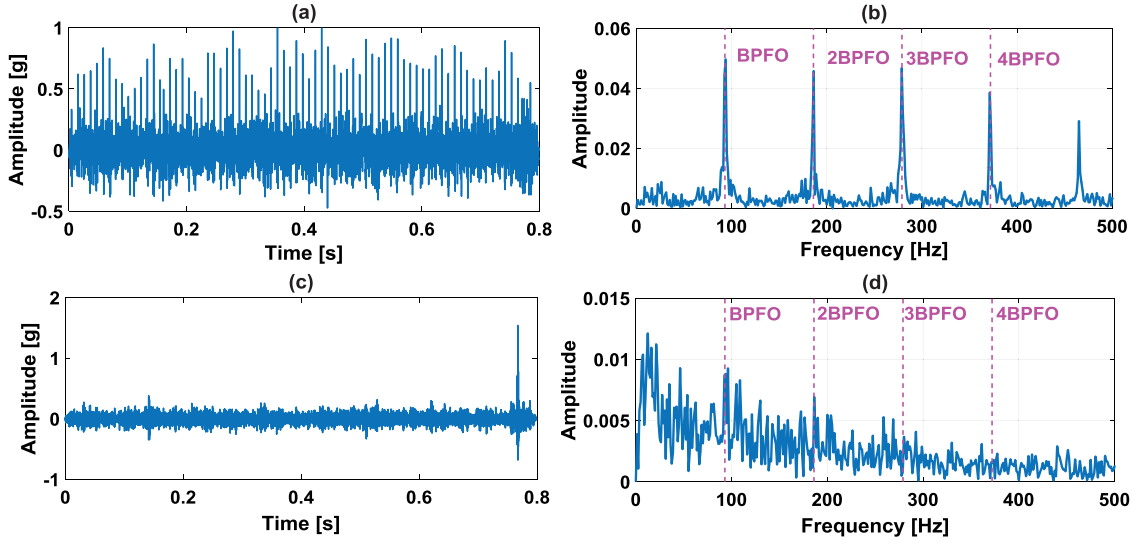


**Fig. 25.** The output results of the outer race fault casing signal at different filter lengths. (a) Time domain waveform, $L = 157$ (optimal); (b) Envelope spectrum of (a); (c) Time domain waveform, $L = 154$; (d) Envelope spectrum of (c).

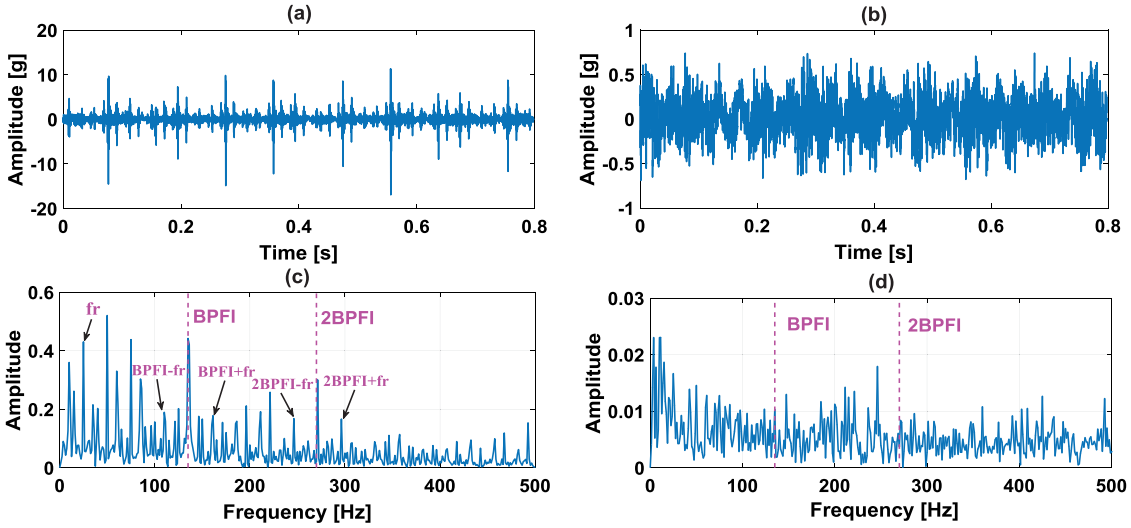


**Fig. 26.** The time domain waveforms and envelope spectra of the inner race fault. (a) Bearing housing; (b) Casing vertical measuring point signal; (c) Envelope spectrum of (a); (d) Envelope spectrum of (b).

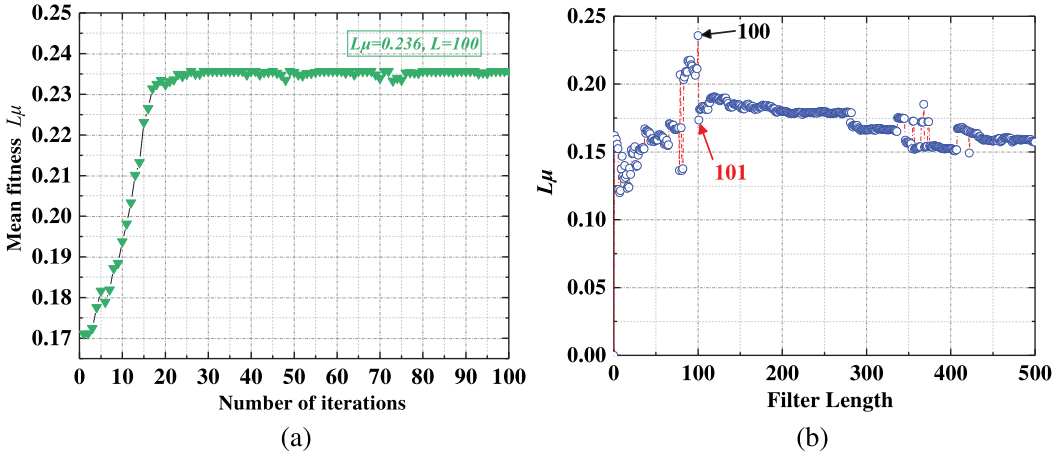


**Fig. 27.** The selection of optimal filter length for casing signal of the inner race fault. (a) Results of GA optimization; (b) The value of $L_\mu$.

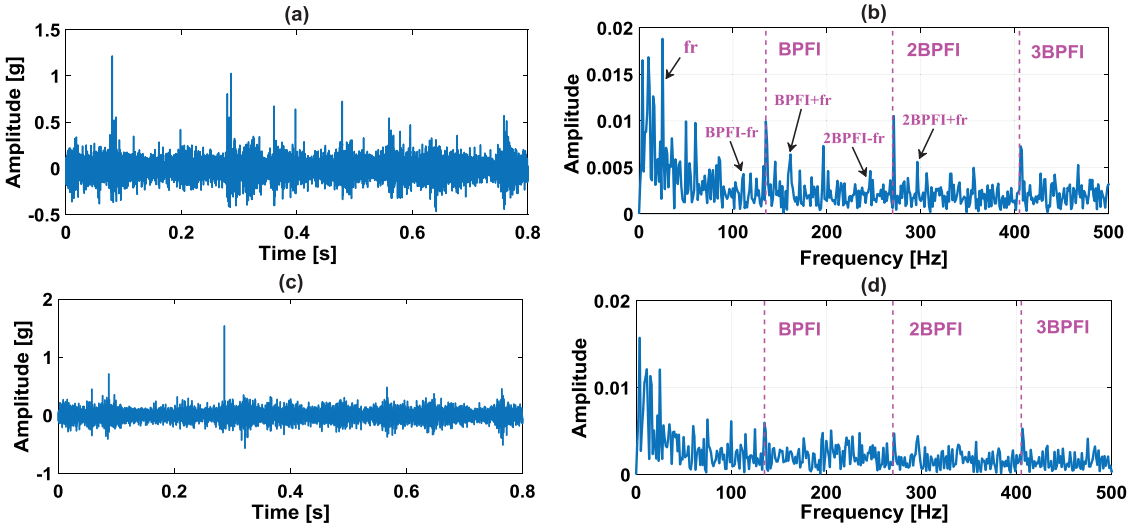


**Fig. 28.** The output results of the inner race fault casing signal at different filter lengths. (a) Time domain waveform, $L = 100$ (optimal); (b) Envelope spectrum of (a); (c) Time domain waveform, $L = 101$; (d) Envelope spectrum of (c).

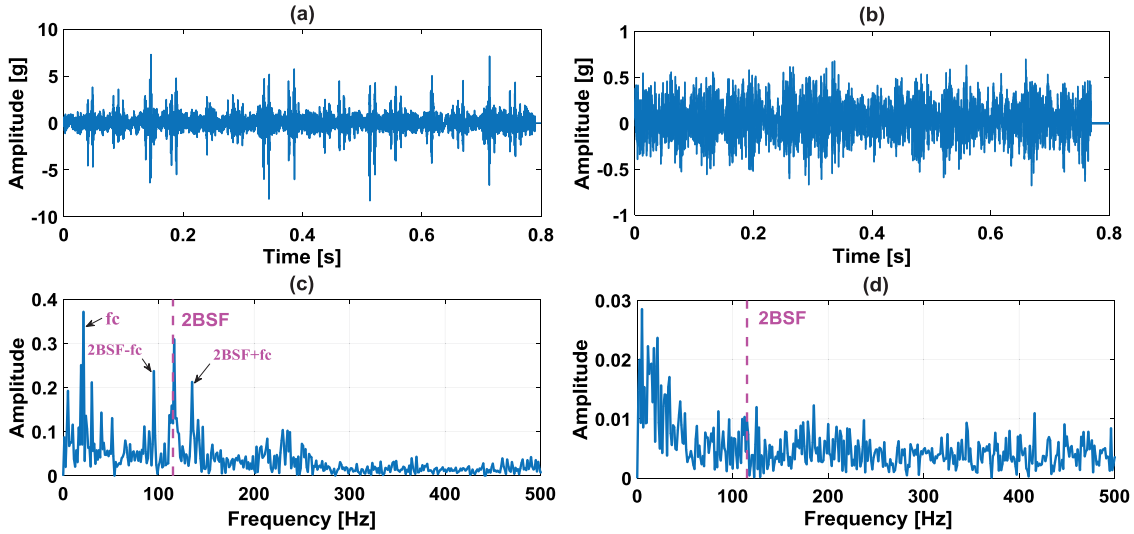


**Fig. 29.** The time domain waveforms and envelope spectra of the ball fault. (a) Bearing housing; (b) Casing vertical measuring point signal; (c) Envelope spectrum of (a); (d) Envelope spectrum of (b).

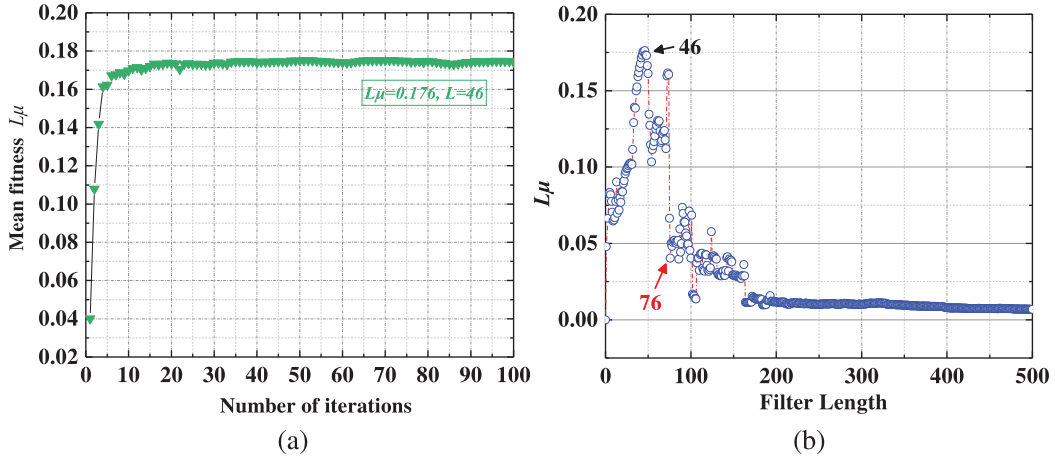


**Fig. 30.** The selection of optimal filter length for casing signal of the ball fault. (a) Results of GA optimization; (b) The value of $L_\mu$.

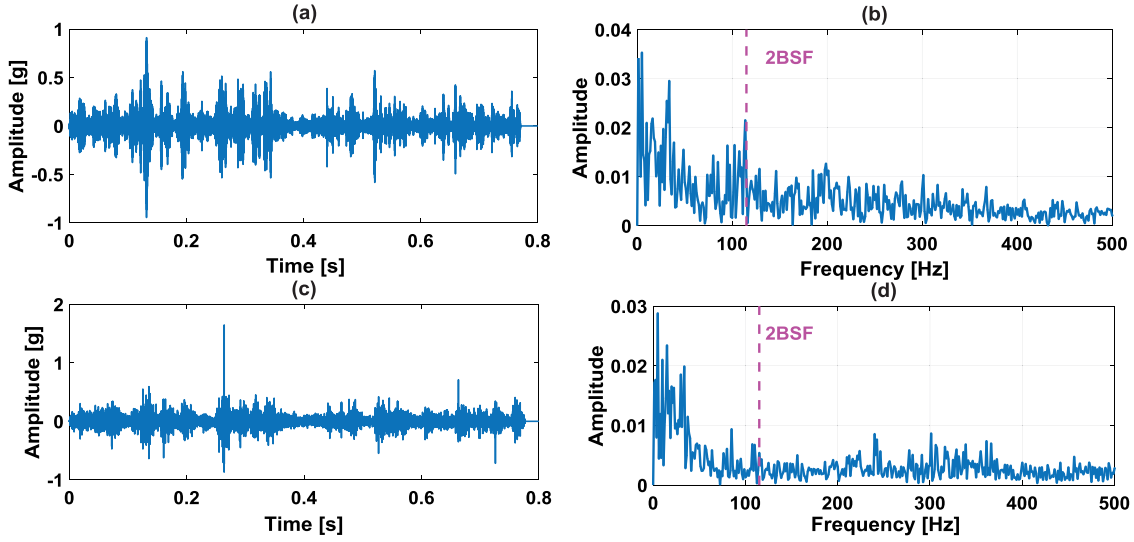


**Fig. 31.** The output results of the ball fault casing signal at different filter lengths. (a) Time domain waveform, $L = 46$ (optimal); (b) Envelope spectrum of (a); (c) Time domain waveform, $L = 76$; (d) Envelope spectrum of (c).

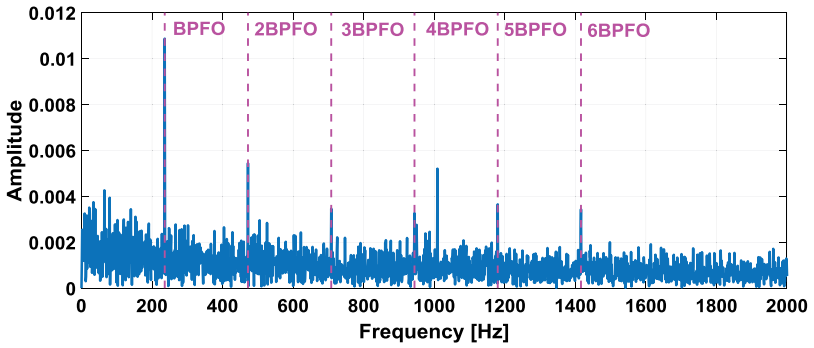


**Fig. 32.** The envelope spectrum of 533 record processed by PSO-MED.

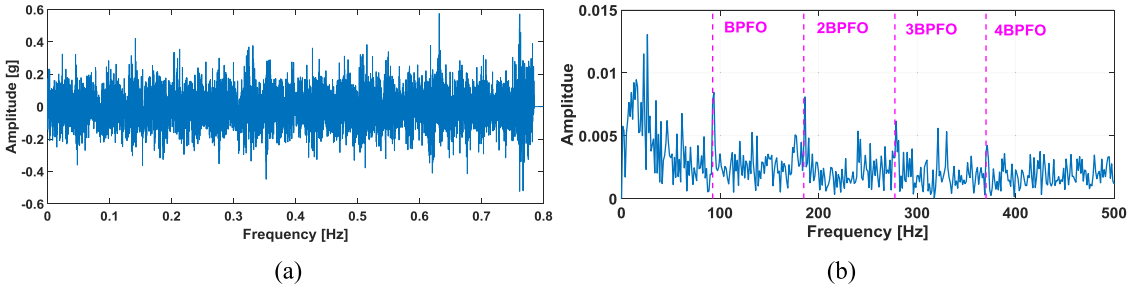


**Fig. 33.** The output of the outer race fault casing signal processed by PSO-MED. (a) Time domain waveform; (b) Envelope spectrum of (a).

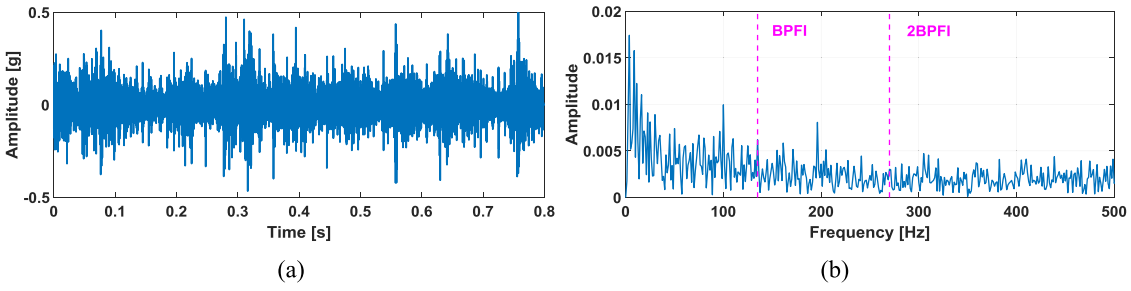


**Fig. 34.** The output of the inner race fault casing signal processed by PSO-MED. (a) Time domain waveform; (b) Envelope spectrum of (a).

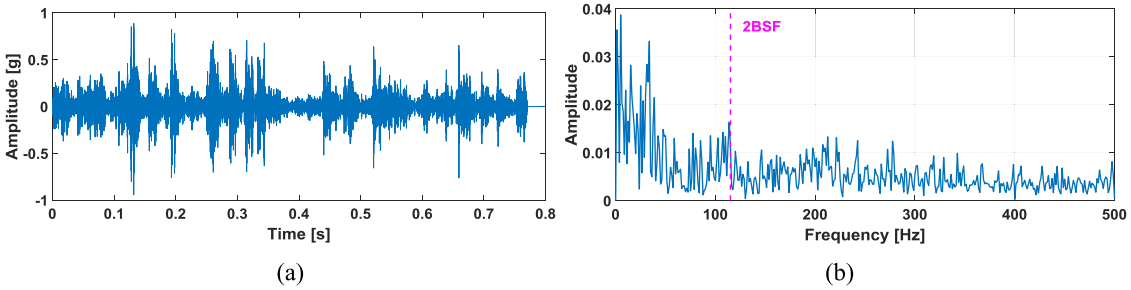


**Fig. 35.** The output of the ball fault casing signal processed by PSO-MED. (a) Time domain waveform; (b) Envelope spectrum of (a).

in diagnosing the casing signals. Fig. 33 is the detection results of the outer race fault casing signal processed by PSO-MED. From the time domain waveform of Fig. 33(a), there is no continuous periodic impulse compared with Fig. 25(a). Although the BPFO and its harmonics can be seen in Fig. 33(b), there are filled with other noise frequencies and the fault features are very weak compared with the results in Fig. 25(b). As for the casing signal of the inner race fault, the results are shown in Fig. 34. It can be observed that there are some prominent impulses in Fig. 34(a). Nevertheless, BPFI and 2BPFI are not observable in Fig. 34(b). The same situation occurs in the detection results of ball fault as shown in Fig. 35. These above results indicate that PSO-MED is not satisfactory in detecting signals that far away from the fault source.

### 5.2. Comparison with MCKD

Maximum correlated kurtosis deconvolution (MCKD) was proposed by McDonald et al. [9]. Based on MED, the main idea of the MCKD is to transform the kurtosis objective function into the correlation kurtosis (CK) objective function to enhance the fault impulses of a specific period. The most sensitive parameter in

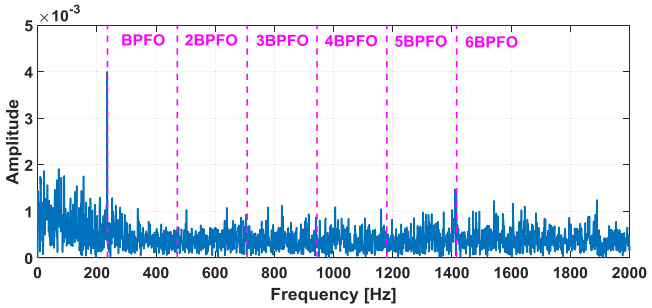


**Fig. 36.** The envelope spectrum of 533 record processed by MCKD.

MCKD is the fault period $T$. An inaccurate $T$ will generate the periodic impulses which are unrelated to the fault and interfere with the diagnosis results. Therefore, to make it fair and ensure that MCKD can get the best results, the parameter $T$ is the corresponding bearing fault characteristic period, that is $T = f_s/\text{BPFO}$ (or BPFI, 2BSF). $f_s$ is the sampling frequency. For 533 record, $T$ is 86.7. For the casing signals, the $T$ of outer race fault is 111.3. The $T$ of inner race fault is 75.8 and the $T$ of ball fault is 89. Additionally, shift order $M$ is 5 and all the signals are filtered at the same optimal filter length as MED.

Fig. 36 is the envelope spectrum of 533 record processed by MCKD. We can see that MCKD can extract BPFO, but it is limited in the extraction of harmonic fault features. The time domain waveform of outer race fault casing signal after MCKD filtered and its envelope spectrum is presented in Fig. 37(a) and Fig. 37(b), respectively. Compared with the result in Fig. 25, the fault impulse characteristics are not obvious in the time domain and there are still some noise frequencies on the spectrum. Nevertheless, it is better than the result of PSO-MED in Fig. 33. Fig. 38 plots the results of inner race fault casing signal filtered by MCKD. We can observe Fig. 38(b) that BPFI has only one weak peak and no harmonics or rotation modulation. And in the result of the ball fault casing signal, the fault feature cannot be found as shown in Fig. 39. From the above results, MCKD is not as effective as the proposed method in this paper when diagnosing the casing signal.

To quantitatively illustrate the advantages of the proposed method, an index named as the characteristic frequency of the envelope (*cfe*) is used to confirm the superiority of the proposed method. This index has a good ability to distinguish fault levels. And similar indexes were used to evaluate the detection ability of their proposed methods in the Refs. [11,14]. *cfe* is calculated as follows:

$$cfe = \frac{\frac{1}{M}\cdot\sum_{i=1}^{M} A\left(i\cdot f_{\text{fault}}\right)}{\frac{1}{N}\cdot\sum_{i=1}^{N} A\left(f_i\right)} = \frac{N\cdot\sum_{i=1}^{M} A\left(i\cdot f_{\text{fault}}\right)}{M\cdot\sum_{i=1}^{N} A\left(f_i\right)}$$

where $A(f)$ is the amplitude at the frequency $f$ in the envelope spectrum. $f_{\text{fault}}$ denotes the fault frequency. $M$ is the multiple of $f_{\text{fault}}$ and its value in this paper is set as 3. $N$ is the number of spectral lines in the envelope spectrum. In the calculation process, the search bandwidth based $f_{\text{fault}}$ is $[-5, 5]$ Hz and $N$ is 500. Fig. 40 shows the quantitative comparison of *cfe* between the proposed method with PSO-MED and MCKD. It can be summarized as follows:

(1) The fault characteristics of the bearing housing signals are very strong. However, the fault characteristics of the casing signal have a serious attenuation because of the transmission path. Besides, among the three fault modes, the outer race fault is the strongest, while the ball fault is the weakest.

(2) The proposed method eliminates the influence of the transmission path and recovers the fault characteristics of the casing signals well. Its detection ability is close to the result of direct signal detection of bearing housing. Compared with PSO-MED and MCKD, the proposed method has obvious advantages in the detection of casing signals.

## 6. Discussions

MED is a classical method in blind deconvolution, but it is essentially a finite impulse response (FIR) filter, so it is necessary to determine its filter length before using it. From the simulation signal and test signals, even if the value of filter length is only 1 different, it will produce completely different outputs. It can be seen that the filter lengths have a great effect on the MED filter results. Although some researches [7–14] are devoted to

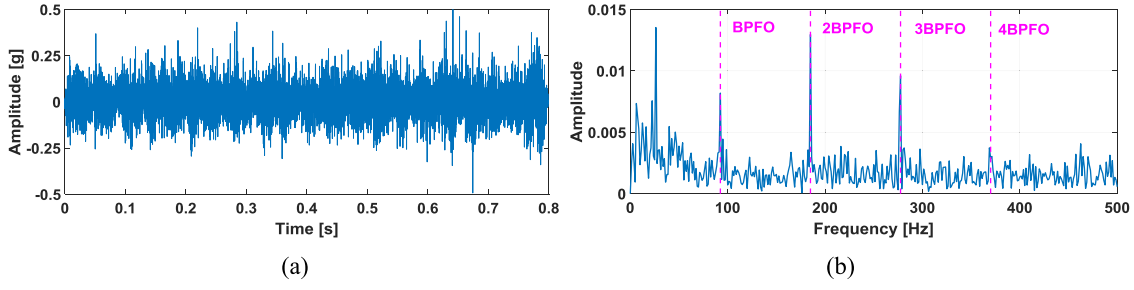


**Fig. 37.** The output of the outer race fault casing signal processed by MCKD. (a) Time domain waveform; (b) Envelope spectrum of (a).

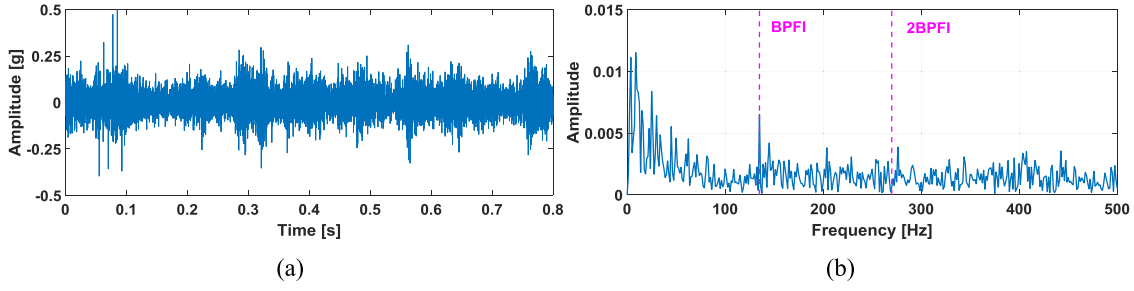


**Fig. 38.** The output of the inner race fault casing signal processed by MCKD. (a) Time domain waveform; (b) Envelope spectrum of (a).

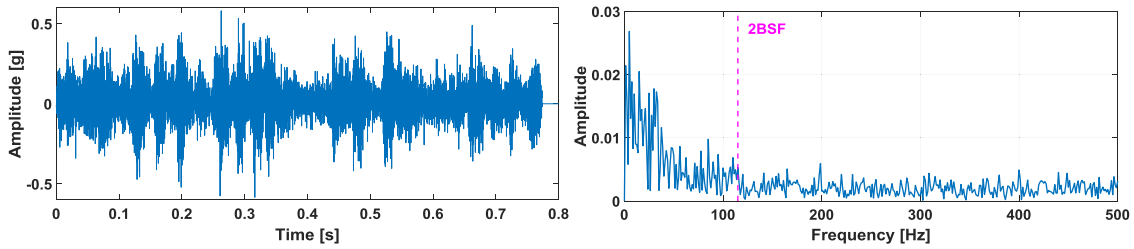


**Fig. 39.** The output of the ball fault casing signal processed by MCKD. (a) Time domain waveform; (b) Envelope spectrum of (a).

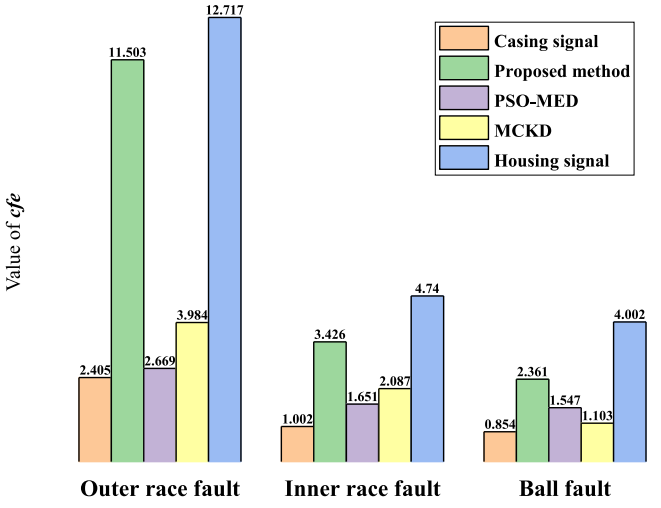


**Fig. 40.** The *cfe* index of three failure modes of fault signals under different cases.

improving the MED and have achieved significant results, these methods also need to set the filter length in advance. Therefore, we believe that the selection of filter length should not be ignored. The core idea of this paper is to establish an index $L_\mu$ that can measure the impact characteristics of periodic fault to evaluate the MED-filtered output signal and avoid the single pulse as much as possible. And this impulse measurement idea is also reflected in the literature [31]. The results of 533 record in the run-to-failure test show that choosing filter length by experience is likely to cause misdiagnosis and yet the proposed method can accurately extract the early bearing fault features. The results of the casing signals show that the interference of the transmission path can be eliminated at the optimal filter length.

PSO-MED aims at the filter coefficients and searches for a set of filter coefficients that can make the signal kurtosis maximum in a certain dimension. However, the filter coefficients are a set of sequences generated by random particles, from which PSO-MED only selects an "optimal solution". It lacks the iterative update of filter coefficients themselves (Eq. (6)), which makes it underperform in weak casing fault signals. MCKD changed the kurtosis objective function of MED. It is better than PSO-MED in the diagnosis results of the casing signal, but it performed badly in the harmonic identification of 533 record. Besides, MCKD relies heavily on the prior fault period $T$. If changing the $T$ of the outer race fault casing signal to 114, the result will be worse as shown in Fig. 41(a). The filter length in MCKD is not primary, because in the case of a given $T$, the larger the filter length is, the better the period $T$ of output is, even if $T$ is not a bearing fault period. Fig. 41(b) depicts the result of the outer race fault casing signal when $T$ is 200 (51.2 Hz) and the filter length is 1000. The result shows that the spectrum has completely become the harmonics of the $T$ (51.2 Hz) period, which indicates that using MCKD may cause misdiagnosis if there is no fault period impulse in the signal. In addition, too large a filter length will make MCKD lose the significance of objective diagnosis.

In Refs. [13,16], an empirical formula Eq. (15) is given to determine the filter length range, where $f_c$ is the resonance frequency of fault excitation. $f_s$ is the sampling frequency of the raw signal. Take the inner race fault casing as an example. As shown in Fig. 42, the resonance peaks $f_c$ is about 1195 Hz (1195–1060 = 135 Hz or 1331–1195 = 136 Hz), $f_s$ = 10.24 kHz. The filter length determined by Eq. (15) is $L > 9$. Obviously, the results of this range cannot meet the requirement of precise optimal filtering.

$$L > \frac{2f_s}{f_c} \tag{15}$$

## 7. Conclusions

This paper presents a method for selecting the optimal filter length of MED which is beneficial to improve the accuracy of MED in the processing of weak impact signals. By combining the autocorrelation function, an energy index is proposed. The index is used as the objective function and substituted into the genetic algorithm to optimize the filter length globally in order to avoid the case that the periodic impulses are enhanced into a single random large pulse at the inappropriate filter length. And two

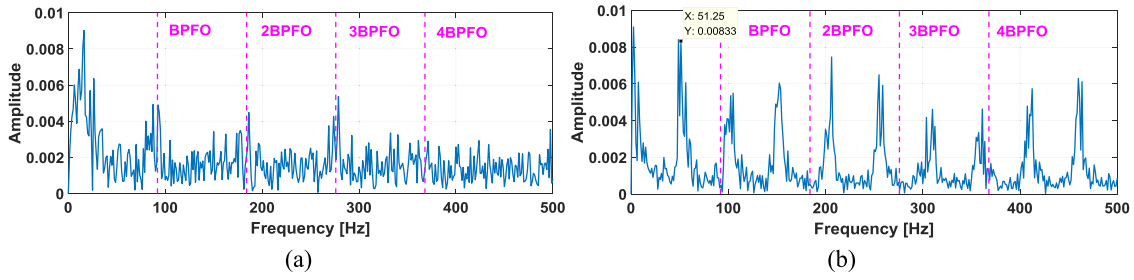


**Fig. 41.** The results of outer race fault casing signal at different prior period $T$. (a) $T$ = 114; (b) $T$ = 200.

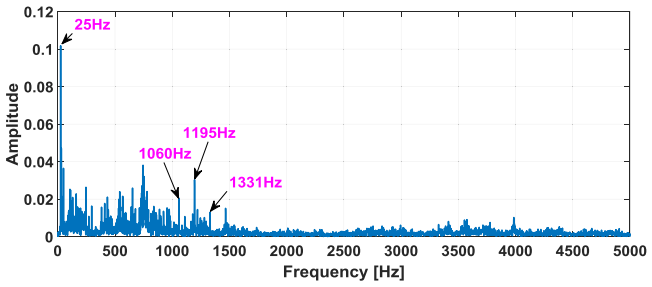


**Fig. 42.** The spectrum of the inner race fault casing signal.

different bearing fault experiments verify the effectiveness of the proposed method. The advantages of the proposed method can be summarized as follows:

(1) The results of the run-to-failure bearing test show that the filter length selected by experience is easy to produce a wrong result in the diagnosis process and the method proposed in this paper can avoid this problem.

(2) The fault casing signal that far away from the bearing vibration source indicate that the transmission path seriously weakens the fault characteristics. The proposed method can eliminate the effect of the transmission path and enhance the weak periodic impulses.

(3) The comparisons with PSO-MED and MCKD indicate that the proposed method has better performance in detecting the weak fault casing signal.

## Declaration of competing interest

The authors declare that they have no known competing financial interests or personal relationships that could have appeared to influence the work reported in this paper.

## Acknowledgments

The first author would like to thank Mohan Yang and Chao He for their help in drawing Fig. 22. This work is supported by the Postgraduate Research & Practice Innovation Program of Jiangsu Province (KYCX20_0211), National Natural Science Foundation of China (No. 51675263), and National Science and Technology Major Project (2017-IV-0008-0045), which are highly appreciated by the authors. The authors would also like to thank the IMS center for the run-to-failure bearing data.

## References

[1] Randall RB, Antoni J. Rolling element bearing diagnostics - A tutorial. Mech Syst Signal Process 2011;25:485–520. http://dx.doi.org/10.1016/j.ymssp.2010.07.017.

[2] Wiggins RA. Minimum entropy deconvolution. Geoexploration 1978;16:21–35. http://dx.doi.org/10.1016/0016-7142(78)90005-4.

[3] Sawalhi N, Randall RB, Endo H. The enhancement of fault detection and diagnosis in rolling element bearings using minimum entropy deconvolution combined with spectral kurtosis. Mech Syst Signal Process 2007;21(6):2616–33. http://dx.doi.org/10.1016/j.ymssp.2006.12.002.

[4] Endo H, Randall RB. Enhancement of autoregressive model based gear tooth fault detection technique by the use of minimum entropy deconvolution filter. Mech Syst Signal Process 2007;21:906–19. http://dx.doi.org/10.1016/j.ymssp.2006.02.005.

[5] Gao YD, Karimi M, Kudreyko AA, Song WQ. Spare optimistic based on improved ADMM and the minimum entropy deconvolution for the early weak fault diagnosis of bearings in marine systems. ISA Trans 2018;78:98–104. http://dx.doi.org/10.1016/j.isatra.2017.12.021.

[6] Wang SH, Xiang JW, Tang HS, Liu XY, Zhong YT. Minimum entropy deconvolution based on simulation-determined band pass filter to detect faults in axial piston pump bearings. ISA Trans 2019;88:186–98. http://dx.doi.org/10.1016/j.isatra.2018.11.040.

[7] Ovacıklı AK, Pääjärvi P, LeBlanc JP, Carlson JE. Recovering periodic impulsive signals through skewness maximization. IEEE Trans Signal Process 2016;64:1586–96, http://ieeexplore.ieee.org/stamp/stamp.jsp?tp=&arnumber=7332952&isnumber=7404064.

[8] Obuchowski J, Zimroz R, Wyłomańska A. Blind equalization using combined skewness–kurtosis criterion for gearbox vibration enhancement. Measurement 2016;88:34–44. http://dx.doi.org/10.1016/j.measurement.2016.03.034.

[9] McDonald GL, Zhao Q, Zuo MJ. Maximum correlated kurtosis deconvolution and application on gear tooth chip fault detection. Mech Syst Signal Process 2012;33:237–55. http://dx.doi.org/10.1016/j.ymssp.2012.06.010.

[10] McDonald GL, Zhao Q. Multipoint optimal minimum entropy deconvolution and convolution fix: application to vibration fault detection. Mech Syst Signal Process 2016;82:461–77. http://dx.doi.org/10.1016/j.ymssp.2016.05.036.

[11] Cheng Y, Chen BY, Mei GM, Wang ZW, Zhang WH. A novel blind deconvolution method and its application to fault identification. J Sound Vib 2019;460:114900. http://dx.doi.org/10.1016/j.jsv.2019.114900.

[12] Zheng K, Luo JF, Zhang Y, Li TL, Wen JF, Xiao H. Incipient fault detection of rolling bearing using maximum autocorrelation impulse harmonic to noise deconvolution and parameter optimized fast EEMD. ISA Trans 2019;89:256–71. http://dx.doi.org/10.1016/j.isatra.2018.12.020.

[13] Cheng Y, Zhou N, Zhang WH, Wang ZW. Application of an improved minimum entropy deconvolution method for railway rolling element bearing fault diagnosis. J Sound Vib 2018;425:53–69. http://dx.doi.org/10.1016/j.jsv.2018.01.023.

[14] Jiang XX, Cheng X, Shi JJ, Huang WG, Shen CQ, Zhu ZK. A new l0-norm embedded MED method for roller element bearing fault diagnosis at early stage of damage. Measurement 2018;127:414–24. http://dx.doi.org/10.1016/j.measurement.2018.06.016.

[15] Tomasz B, Sawalhi N. Fault detection enhancement in rolling element bearings using the minimum entropy deconvolution. Arch Acoust 2012;37:131–41. http://dx.doi.org/10.2478/v10168-012-0019-2.

[16] Miao YH, Zhao M, Lin J, Lei YG. Application of an improved maximum correlated kurtosis deconvolution method for fault diagnosis of rolling element bearings. Mech Syst Signal Process 2017;92:173–95. http://dx.doi.org/10.1016/j.ymssp.2017.01.033.

[17] Li JM, Li M, Zhang JF. Rolling bearing fault diagnosis based on time-delayed feedback monostable stochastic resonance and adaptive minimum entropy deconvolution. J Sound Vib 2017;401:139–51. http://dx.doi.org/10.1016/j.jsv.2017.04.036.

[18] Abboud D, Elbadaoui M, Smith WA, Randall RB. Advanced bearing diagnostics: a comparative study of two powerful approaches. Mech Syst Signal Process 2019;114:604–27. http://dx.doi.org/10.1016/j.ymssp.2018.05.011.

[19] Zhang L, Hu NQ. Fault diagnosis of sun gear based on continuous vibration separation and minimum entropy deconvolution. Measurement 2019;141:332–44. http://dx.doi.org/10.1016/j.measurement.2019.04.049.

[20] He D, Wang XF, Li SC, Lin J, Zhao M. Identification of multiple faults in rotating machinery based on minimum entropy deconvolution combined with spectral kurtosis. Mech Syst Signal Process 2016;81:235–49. http://dx.doi.org/10.1016/j.ymssp.2016.03.016.

[21] Li G, Zhao Q. Minimum entropy deconvolution optimized sinusoidal synthesis and its application to vibration based fault detection. J Sound Vib 2017;390:218–31. http://dx.doi.org/10.1016/j.jsv.2016.11.033.

[22] Holland JH. Adaptation in natural and artificial systems. Ann Arbor, MI: University of Michigan Press; 1975.

[23] Goldberg DE. Genetic algorithm in search, optimization and machine learning, vol. 7. Addison Wesley xiii; 1989, p. 2104–16.

[24] Mohd YH, Darus IZM, Hadi MS. Modeling of flexible manipulator structure using genetic algorithm with parameter exchanger. In: Fifth international conference on computational intelligence. IEEE; 2019, http://dx.doi.org/10.1109/CIMSim.2013.15.

[25] Jadhav S, He HM, Jenkins K. Information gain directed genetic algorithm wrapper feature selection for credit rating. Appl Soft Comput 2018;69:541–53. http://dx.doi.org/10.1016/j.asoc.2018.04.033.

[26] Samanta B, Al-Balushi KR, Al-Araimi SA. Artificial neural networks and support vector machines with genetic algorithm for bearing fault detection. Eng Appl Artif Intell 2003;16:657–65. http://dx.doi.org/10.1016/j.engappai.2003.09.006.

[27] Guan XY, Chen G. Sharing pattern feature selection using multiple improved genetic algorithms and its application in bearing fault diagnosis. J Mech Sci Technol 2019;33:129–38. http://dx.doi.org/10.1007/s12206-018-1213-6.

[28] Zhou M, Sun SD. Genetic algorithms: theory and applications. Beijing: National Defense Industry Press; 1999 ([in Chinese].

[29] Qiu H, Lee J, Lin J, Yu G. Wavelet filter-based weak signature detection method and its application on rolling element bearing prognostics. J Sound Vib 2006;289:1066–90. http://dx.doi.org/10.1016/j.jsv.2005.03.007.

[30] Mei GM. Data for a novel blind deconvolution method and its application to fault identification, Mendeley Data, v1; 2019. http://dx.doi.org/10.17632/787s5xvsgh.1.

[31] Zhao M, Jia XD. A novel strategy for signal denoising using reweighted SVD and its applications to weak fault feature enhancement of rotating machinery. Mech Syst Signal Process 2017;94:129–47. http://dx.doi.org/10.1016/j.ymssp.2017.02.036.